Emerging trends in 2D nanotechnology that are redefining our understanding of "Nanocomposites"

As Published: 10.1016/J.NANTOD.2018.04.012

Publisher: Elsevier BV

Persistent URL: https://hdl.handle.net/1721.1/135036

Version: Author's final manuscript: final author's manuscript post peer review, without publisher's formatting or copy editing

Nano Today xxx (2018) xxx–xxx

Contents lists available at ScienceDirect

Nano Today

journal homepage: www.elsevier.com/locate/nanotoday

Review

Emerging trends in 2D nanotechnology that are redefining our understanding of "Nanocomposites"

Pingwei Liu[a,b], Anton L. Cottrill[b], Daichi Kozawa[b], Volodymyr B. Koman[b], Dorsa Parviz[b], Albert Tianxiang Liu[b], Jingfan Yang[b], Thang Q. Tran[c], Min Hao Wong[b], Song Wang[a], Michael S. Strano[b,*]

[a] State Key Lab of Chemical Engineering, College of Chemical and Biological Engineering, Zhejiang University, Hangzhou 310027, China
[b] Department of Chemical Engineering, Massachusetts Institute of Technology, Cambridge, MA 02141, USA
[c] Department of Mechanical Engineering, National University of Singapore, 9 Engineering Drive 1, EA-07-05, Singapore 117575, Singapore

ARTICLE INFO

Article history:
Received 10 November 2017
Received in revised form 3 April 2018
Accepted 19 April 2018
Available online xxx

Keywords:
Nanotechnology
2D materials
Graphene
Polymers
Nanocomposites
Hybrids
Nanofillers
Fibers
Mechanical reinforcement
Multifunctional composites
Barrier properties
Electrical conduction
Thermal conduction
Optical properties
Liquid-exfoliation
Chemical vapor deposition
Folding
Multilayer

ABSTRACT

The goal of this review is to summarize the recent development of nanocomposites of 2D materials, especially polymer nanocomposites with large-area, high-quality 2D sheets, and more importantly, the future direction of this field. Scientists and engineers have a tendency to review and envision the future based on the past, but innovation does not work like this. Herein, we do not provide a comprehensive review of nanocomposites with 2D materials; rather, we highlight unusual or unconventional directions emerging for nanocomposite materials research. This forward-looking perspective of current trends focuses on new research directions. In this review, we summarize the fundamentals of nanocomposites in regards to the mechanical and functional reinforcement at the theoretical limit, and we briefly introduce the synthesis of large-area 2D materials with high quality and their controlled dispersion into matrix materials to achieve the maximum reinforcement predicted by theory. We continue with the classical and fundamentally important problem of the mechanical reinforcement in nanocomposites; that is, does the reinforcing contribution come from the modification of matrix or the direct mechanical reinforcement by the nanofillers? We present and discuss new forms of nanocomposites with layered and scrolled structure and well-positioned, semi-infinite 2D layers in detail. We also address the functional reinforcement from the continuous 2D sheets and the unusual applications of nanocomposites enabled by these functional 2D layers. In particular, we discuss fiber devices, such as an electromagnetic inductor and a thermal spiral conductor, an atomic-thick barrier film, a bioactive hybrid via attaching 2D layers to a living organism such as plant leaves, intelligent particle devices acting as state machines, and optical devices such as single photon emitters. With these, we further introduce the new nanocomposite concept of a three-dimensional (3D) macroscopic nanocomposite body comprised exclusively of 2D topology. Finally, we discuss the scalability challenges of the production process and the outlook of potential solutions. We hope this review and perspective can intrigue researchers who are currently working in the fields of 2D materials, polymers, and nanocomposites and provide some new insights to promote the future development of nanocomposites.

Contents

* Corresponding author.
E-mail address: strano@mit.edu (M.S. Strano).

https://doi.org/10.1016/j.nantod.2018.04.012
1748-0132/

Introduction

Precise control over every atom and molecule, its position, and chemical interaction with its neighbors is an ultimate goal of material science, which would give access to engineering materials with nanometer precision and versatile properties. Despite our ability to synthesize molecules and nanoparticles, the atomic control via inducing or compositing single atom defects or discontinuities in already-existing materials remains a dream. It remains challenging to position atoms at specific locations and to arrange molecules in desired structures. The emergence of two-dimensional (2D) materials or molecules, however, may help to realize this dream, considering that stacking layers of 2D materials or interfacing/compositing them with other materials is a relatively simple and efficient way to achieve this structural control at an atomic level.

Since the first mechanical exfoliation of a single-layer of graphene from graphite by Geim and Novoselov in 2004 [1], we have experienced a rapid development of two-dimensional (2D) materials in such areas as synthesis, fabrication, characterization, and novel applications [2–6]. The 2D family is expansive. 2D allotropes of various elements including graphene, phosphorene, silicone, germanine, and others, as well as 2D compounds like transition metal dichalcogenides and hexagonal boron nitride, have been experimentally reported (Fig. 1) [6]. These 2D materials have exotic chemical, mechanical, and physical properties as compared to their 3D counterparts. For example, graphene with sp^2-hybridized carbon-carbon bonds has an elastic stiffness approaching 1 TPa and a strength up to 135 GPa [7,8]. Graphene is also electrically and thermally conductive with an outstanding electron mobility of 200,000 $cm^2\ V^{-1}\ s^{-1}$ [9] and measured thermal conductivities in the range from 1500 to 3000 $W{\cdot}m^{-1}{\cdot}K^{-1}$ [10–16]. MoS_2 and phosphorene are semiconductors, while hBN is insulating. A heterojunction of these 2D layers via Van der Waals force can generate new electronic, optical, and optoelectronic devices with various functions such as sensing, actuating, memory, energy harvesting, and storage [17–22], and the device size can be minimized to nanometer-thickness, which is impossible for traditional materials. This makes 2D materials one of the most attractive materials to study in the field of nanotechnology [3,4,23,24] and forms an important branch termed as 2D nanotechnology [3].

In the research of nanomaterials, one of the biggest challenges is scalability [25]. In the field of 2D nanotechnology, we also have to address the same problem: can we translate the superior properties of thin 2D sheets or their heterojunctions found at atomic, nanometer thicknesses, or nanoscale into a macroscopic level? Can we translate the fundamental advances achieved in academic research of 2D materials into tangible technological applications that can make an impact in the real world? One could imagine that to achieve a macroscopic millimeter-thick composite material composed of different 2D layers, we would need to stack roughly one million layers. This number of layers is currently challenging to achieve due to high synthesis price and imperfect transfer processing. A more promising strategy of creating macro materials with 2D layers is hybridizing the latter with other macroscopic layers - specifically, interfacing or compositing 2D materials with bulk matrix materials, such as polymers or metals, with the purpose to use the 2D materials as nanoinlcusions to reinforce these matrixes in terms of mechanical performance and functionalities. In this review, we will demonstrate how minimal inclusions of 2D materials can considerably alter mechanical, electrical, thermal, and optical properties of the matrix composites, and we will limit ourselves to large-area 2D inclusions.

Ultra-thin 2D nanosheets have the unique advantages of a higher surface area and multiple functionalities, which differentiates them from various nanoparticles when constructing novel nanocomposite materials. Most review papers of nanocomposites with 2D materials deal with small-sized nanoflakes exfoliated from bulk-layered materials (Fig. 1), such as small-sized graphene oxides or their derivatives, which are largely available at a relatively low cost. Their quality and various properties, however, are degraded significantly compared to their pristine counterparts due to the introduction of defects and cracks [26–34], which significantly downplay the advantages of 2D nanoinclusions. Also, when commonly dispersed in solvents, 2D material flakes coexist with various surfactants that also alter their properties. Here, our major interest is nanocomposites with large-area 2D sheets of relatively high quality (e.g., 2D sheets produced by chemical vapor deposition (CVD) methods). We will review and discuss their synthesis and dispersion control into polymer matrices for mechanical and functional reinforcement at the theoretical limit, and consequently, address potential applications of these nanocomposites as new materials and devices.

More specifically, we will start with theoretical considerations of the advantages of using large-area 2D materials with high aspect ratio as nanofillers for nanocomposites (*i.e.*, achieving a substantial and maximum reinforcement at a minuscule addition regarding of mechanical properties, barrier performance, electrical and thermal conduction). We will further summarize and discuss: (1) The production of large-area 2D materials, including two major categories

Please cite this article in press as: P. Liu, et al., Emerging trends in 2D nanotechnology that are redefining our understanding of "Nanocomposites", Nano Today (2018), https://doi.org/10.1016/j.nantod.2018.04.012

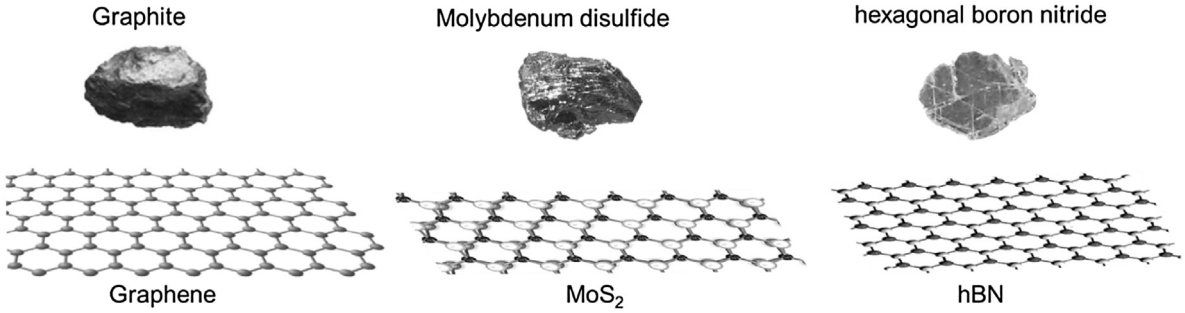

Fig. 1. Several typical 2D materials: graphene, MoS_2, hBN, and their corresponding single crystal bulk materials.

of methods – top-down exfoliation and bottom-up chemical vapor deposition method. (2) The newly emergent processing techniques and methods to disperse and align these large-area 2D sheets into or onto matrix materials to answer the important question of how to achieve an efficient hybridization without compromising the superior properties of these 2D materials. (3) The experimentally achieved mechanical reinforcement and functions in nanocomposites with large-area, continuous 2D materials (we will hereafter term as 2D nanocomposites) and the potential device applications of these 2D nanocomposites as an electromagnetic inductor, a functional barrier, an intelligent particle state machine, a thermal spiral, and a single photon emitter. Finally, we highlight our new nanocomposite concept that *a three-dimensional (3D) composite body comprised exclusively of 2D topology* and the existing challenges and potential solutions to advance this field. With these, we hope this paper, instead of giving a comprehensive and encyclopedic summary of the field, can provide creative perspectives and ideas that can direct the further development of novel nanocomposites enabled by 2D nanotechnology.

Theoretical background

Mechanical reinforcement

Large-area graphene with a higher aspect ratio promises a more efficient mechanical reinforcement. An early study from Robert Young's group found that a continuum mechanics approach is valid for polymer nanocomposites with atomic-thick fillers, such as graphene [31,35]. A variety of micromechanics models can predict the stiffness and strength reinforcement in nanocomposites with graphene [33,36,37]. In a model nanocomposite with monolayer graphene (Fig. 2a) in a matrix, the shear lag theory can predict the shear transfer between the matrix and the graphene filler [31,35,38]. Similar to those short-fiber-reinforced composites, a critical length of the 2D platelet l_c, defined as 2 × the distance over which the strain rises from the platelet edge to the plateau level [31], is about 3 μm for pristine graphene on a polymer support based on a Raman spectroscopy mapping study of stress transfer [35]. The graphene nanoflakes should have a size $>10l_c$, ~ 30 μm, with an aspect ratio (a) ~ 10^5 (the thickness of a monolayer graphene is about 0.34 nm) to achieve a sound reinforcement.

For bulk composites, if the nanoplatelets are well bonded with the matrix and well aligned, the Mori Tanaka model [39,40] (Tandon and Weng's equations, for example [40]) and the Halpin–Tsai model [41] can predict the modulus enhancement. The latter model is empirical and widely used because of its relative simplicity. For nanocomposites with parallel-aligned nanoplatelets (Fig. 2b), this model gives Young's modulus in the longitudinal direction ($E_\parallel$) as:

$$E_\parallel = \left[\frac{1+2\alpha\eta_\parallel v_f}{1-\eta_\parallel v_f}\right] E_m, \quad \text{where } \eta_\parallel = \frac{E_f/E_m - 1}{E_f/E_m + 2\alpha}. \tag{2.1}$$

E_f and E_m are Young's modulus of the nanoplatelets and polymer matrix, respectively. v_f is the volume fraction of the fillers, and a is the aspect ratio of the filler (a = width/thickness). When $a \to \infty$ (Fig. 2c), Eq. (1) gives the maximum reinforcement – the rule of mixtures,

$$E_\parallel = E_f v_f + E_m\left(1 - v_f\right). \tag{2.2}$$

The reinforcement approaches this limit when a >10,000 (Fig. 3a) [43]. The Young's modulus in the transverse direction ($E_\perp$) is insensitive to a,

$$E_\perp = \left[\frac{1+2\eta_\perp v_f}{1-\eta_\perp v_f}\right] E_m, \quad \text{where } \eta_\perp = \frac{E_f/E_m - 1}{E_f/E_m + 2}. \tag{2.3}$$

Using $E_\parallel$ and $E_\perp$, we can calculate the modulus of nanocomposites with 3D randomly oriented nanoplatelets using two coefficients m and n,

$$E_{3D} = mE_\parallel + nE_\perp, \tag{2.4}$$

where m = 0.49 and n = 0.51 approximately based on the laminate theory [44,45].

Barrier performance

Graphene and other 2D materials are good barrier materials. For example, graphene, with high electron-density in its sp^2-bonded aromatic rings, is impermeable to all molecules [46] and only permeable to protons [47], making it the thinnest membrane for liquid/wet biological sample encapsulation at high vacuum and a protective barrier against harsh environments. The compositing of graphene or other 2D sheets with good barrier properties to a polymer matrix will alter the diffusion pathway of molecules and make it tortuous, and thus reduces the gas/vapor permeability. Such a nanocomposite can be used for packaging materials for food, electronics, or other applications. The gas/liquid permeability of the nanocomposite can also be effectively reduced by using fillers with large α [48,49]. For polymer nanocomposites with layered 2D sheets oriented perpendicular to the diffusion path, if these nanoplatelets are dilute and well distributed with a low volume fraction (φ) is < 0.01, the Nielsen approximation can describe the relative permeability (P/P_0) [50]

$$P/P_0 = (1-\varphi)/(1+\alpha\varphi), \tag{2.5}$$

where α is the aspect ratio. Equation 2.5 predicts that the barrier properties of the nanocomposite will be increased significantly at a higher α. When graphene with $\alpha \geq 1000$ is used, a tiny volume fraction of graphene (e.g., 0.0015) can achieve a significantly improved barrier performance ($P/P_0 \approx 0.1$) (Fig. 3b). In addition, these predicated results have been demonstrated experimentally [51]. When the aspect ratio approaches infinity, the required amount of the filler materials to achieve a good barrier property is negligible.

Please cite this article in press as: P. Liu, et al., Emerging trends in 2D nanotechnology that are redefining our understanding of "Nanocomposites", Nano Today (2018), https://doi.org/10.1016/j.nantod.2018.04.012

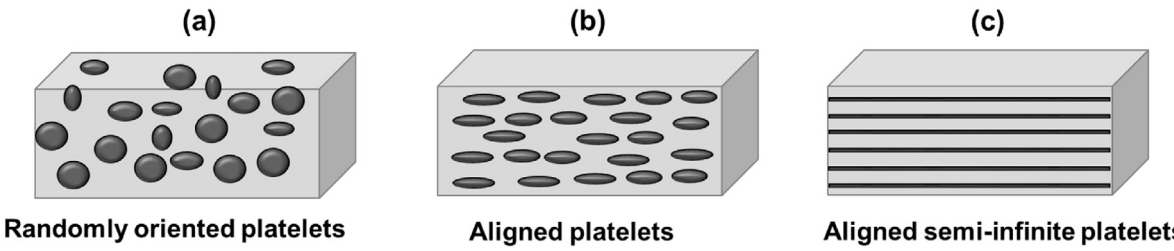

Fig. 2. Nanocomposites with (a) randomly oriented nanoplatelets, (b) aligned platelets, and (c) aligned semi-infinite platelets that span entirely the physical dimension of the composite body.

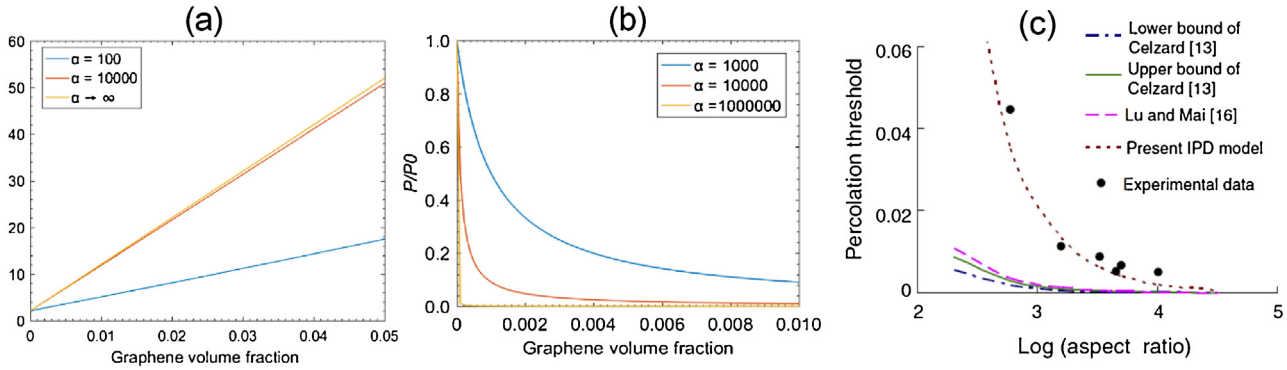

Fig. 3. (a) Mechanical stiffness enhancement (b) barrier properties and (c) percolation threshold of electrical conduction of polymer nanocomposites with graphene at different aspect ratios. Reproduced from with permission from [42]. Copyright (2007) Elsevier.

Electrical conduction

Nanofillers with larger α can significantly reduce the percolation threshold of the nanocomposites [42,52]. The percolation theory can be applied to understand the electrical conductivity of composite materials, which gives the following equations near the percolation threshold with a volume fraction of V_c [53]:

$$\sigma = \sigma_0 \left(V_f - V_c\right)^s, \tag{2.6}$$

where σ is the electrical conductivity of composite, σ_0 is the filler conductivity, V_f is the filler volume fraction, and s is a conductivity exponent. The composite will be conductive once V_f is larger than V_c. Taking nanocomposites with disc-shaped nanoparticles oriented two-dimensionally and randomly as an example, the analytical model developed by Jing Li and Jang-Kyo Kim [42] based on the average interparticle distance (D_{IP}) concept yields the 2D filler volume fraction [54]:

$$V_{f-2D} = \frac{2\pi D^2 t}{(D + D_{IP})^3}, \tag{2.7}$$

If these nanodiscs are oriented randomly in 3D,

$$V_{f-2D} = \frac{27\pi D^2 t}{4(D + D_{IP})^3}, \tag{2.8}$$

where D is the diameter of the disc and t is the thickness of the platelet. When the aspect ratio $D/t \geq 500$, the effect of D_{IP} on V_c becomes negligible. When the aspect ratio ≥ 5000, V_c becomes very small, less than 1% for example, even if the nanoplatelets are randomly oriented in 3D (Fig. 3c).

Thermal conduction

Thermal conduction in an isotropic, two-phase composite with low filler volume fraction is well represented by the well-known Maxwell model, as given in Eq. (2.9). The Maxwell model assumes that the filler particles are spherical, isolated, and randomly distributed within the matrix [55]:

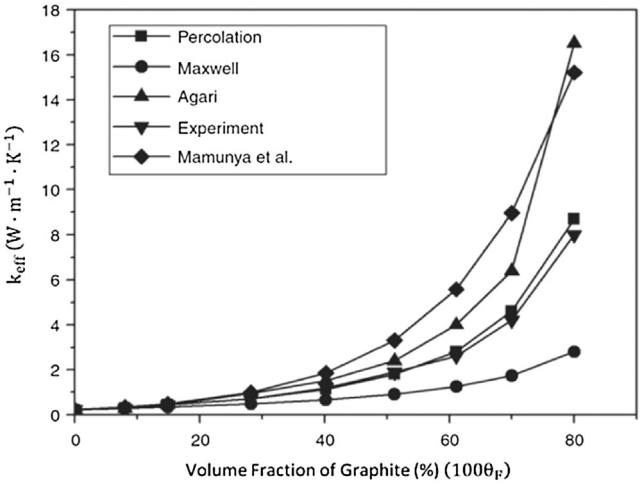

Fig. 4. Results for the effective thermal conductivity of a graphite/PTFE composite as a function of graphite content as obtained from experiment and modeling. Reproduced with permission from [55]. Copyright (2010) SAGE Journals.

$$k_{eff,M} = \frac{2k_M + k_F + 2\theta_F (k_F - k_M)}{2k_M + k_F - \theta_F (k_F - k_M)} k_M, \tag{2.9}$$

where $k_{eff,M}$ is the effective thermal conductivity of the composite predicted by the Maxwell model, k_M is the thermal conductivity of the matrix, k_F is the thermal conductivity of the filler, and θ_F is the volume fraction of filler.

Considering a graphite/polytetrafluoroethylene (PTFE) composite, the Maxwell model adequately predicts the experimental thermal conductivity of the composite at low graphite filler concentrations (Fig. 4) [55]. However, the Maxwell model inadequately describes the experimental thermal conductivity of the compos-

ite at graphite concentrations above approximately 30 vol percent. Shahil and Balandin investigated the effective thermal conductivity of multilayer graphene/epoxy composites in the regime of low graphene volume fractions, and their data were also well-represented by a Maxwell model (Maxwell-Garnett effective medium approximation) [56]. To illustrate the size effects of the graphene in this low concentration regime, the researchers described the graphene filler thermal conductivity according to kinetic theory, as shown in Eq. (2.10).

$$k_F = \frac{1}{3} C v \Lambda_{eff}, \tag{2.10}$$

where C is the volumetric specific heat, v is the phonon group velocity, and Λ_{eff} is the effective phonon mean free path, as obtained from Matthiesssen's rule in Eq. (2.11).

$$\frac{1}{\Lambda_{eff}} = \frac{1}{\Lambda_b} + \frac{1}{L}, \tag{2.11}$$

where Λ_b is the bulk phonon mean free path and L is the size of the graphene flake [56]. From Eq. (2.11), we can deduce that larger graphene flakes will result in a larger effective mean free phonon path and a larger filler thermal conductivity, due to reduced phonon scattering at the graphene flakes' boundaries. In turn, the larger filler thermal conductivity will enhance the effective thermal conductivity of the composite in the low concentration regime described by the Maxwell model.

As shown in Fig. 4, the validity and accuracy of the Maxwell model breaks down as the filler volume fraction exceeds the dilute limit. Depending on the thermal conductivity discrepancy between the matrix and filler materials, percolation theory, as discussed previously in the section on electrical conduction, may or may not apply to predicting the effective thermal conductivity of the composite [55]. Application of percolation theory for thermal conduction can be problematic because, in contrast to electrical conduction, the matrix is often capable of sufficiently transporting heat. The electrical conductivity of the filler is often 10^{10}-10^{20} times larger than that of the matrix in composites, while the thermal conductivity typically does not exceed 10^3, as noted by Zhang et al. [55]. Therefore, the application of percolation theory may not always apply to a two-phase composite with a high thermally conducting filler material, as some authors have reported [55]. However, for the graphite/PTFE system shown in Fig. 4, percolation theory adequately describes the experimental data ($k_F = 135\,W\,m^{-1}\,K^{-1}$; $k_M = 0.22\,W\,m^{-1}\,K^{-1}$) and should adequately describe a highly thermally conductive 2D material such as graphene in a polymeric matrix. Therefore, for a randomly oriented two phase composite consisting of a highly conductive 2D filler and a polymeric matrix, the effective thermal conductivity of the composite can be predicted by Eq. (4) across various filler concentration regimes. Also, the conclusions based on the area of the 2D nanomaterial that was drawn in the section on electrical conduction can also be applied to the thermal properties of the system.

$$k_{eff,P} = k_F \left(\frac{k_c}{k_F}\right)^{\left[\frac{1-\theta_F}{1-\theta_c}\right]^n} \tag{2.12}$$

where $k_{eff,P}$ is the effective thermal conductivity predicted by the percolation model, k_c is the thermal conductivity at the percolation threshold (θ_c), and n is the percolation exponent [55].

The production of large-area 2D materials with high quality

The production of continuous, large-area 2D materials with controlled layer thickness, high quality, and a low number of defects is an ever-increasing area, which has received a lot of attention [1,57–64]. Since many review papers have addressed this topic, we will not give a comprehensive review and discussion pertaining to it. For the convenience of readers who may not work in this field, we will still present a summary of the two major methods used to obtain large-area, high-quality 2D materials, namely, the top-down exfoliation and the bottom-up chemical vapor deposition.

Top-down synthesis via exfoliation

Single-layer graphene was the first member of the 2D nanomaterials family that was exfoliated from parent graphite via micromechanical cleavage (also known as the scotch-tape method) [1]. Although this method produces high-quality pristine graphene nanosheets, it suffers from low yield and a lack of scalability. The main obstacle to the exfoliation of nanosheets in bulk quantities is the strong attractive forces (i.e., van der Waals (vdW)) between the layers of the parent material that resist against their separation and stabilization. This energy barrier can be overcome using an external force in various forms, including mechanical and electrochemical. Methods such as sonication, shear mixing, and ball milling, as well as electrochemical exfoliation, have been used to produce large quantities of the nanosheets in a scalable manner in both solid and liquid phases [65–68]. Pre-treatment of the parent materials to increase the interlayer spacing can improve the efficiency of exfoliation [69]. Stability of the exfoliated nanosheets, particularly in the liquid phase, is another important issue that can affect their yield and also their further applications. Nanosheets are prone to aggregation after the exfoliation due to the attractive vdW forces. Various strategies have been applied to stabilize these nanosheets in the liquid phase and or facilitate their re-dispersion in the liquid phase after exfoliation in the solid phase. Using dispersion media with surface energies similar to that of the nanosheets, as well as covalent and non-covalent functionalization of nanosheets are the main methods to achieve colloidal stability in the nanosheet dispersion [65,70–72]. Production of nanosheets via exfoliation may be categorized based on the methods of pre-treatment for the parent materials, exfoliation techniques, and stabilization strategies applied to these materials. Fig. 5 demonstrates the main three methods that have been applied for the production of bulk quantities of nanosheets thus far. Here, we briefly discuss each of these approaches. More details of the production of 2D materials can be found in several review papers [6,73], and here we are mainly interested in the production of a large-area 2D thin sheet with high quality.

The direct exfoliation of nanosheets is the most straightforward method to produce these materials. In this approach, mechanical force is exerted on the parent materials via sonication [65], shear mixing [66], ball milling [67], or thermal expansion [74] to exfoliate single-, few-, and multi-layers of nanosheets. After exfoliation, the non-exfoliated materials should be separated from the exfoliated and stable nanosheets via the appropriate centrifugation process to assure the quality of the product. Usage of solvents with surface energies similar to the nanosheets (e.g., NMP or DMF) as the dispersion medium facilitates the exfoliation via minimization of the surface tension at the nanosheets-solvent interface [65,75]. This approach prevents the immediate aggregation of exfoliated nanosheets and guarantees their colloidal stability and uncompromised quality. However, most of such solvents have a high-boiling point and are toxic. Thus, the complete removal of the solvent and the residual solvent content of the products becomes an issue for further applications of the nanosheets. In an alternative approach, the nanosheets are exfoliated in the presence of hydrophilic dispersant compounds in aqueous media. The dispersants, which are usually surfactants [72,76], polymers [77] and small aromatic-based molecules [78,79], non-covalently functionalize nanosheets and provide an electrostatic and/or steric shield around the nanosheets to prevent the aggregation. Using this approach, aqueous dispersions of the nanosheets with concentra-

Please cite this article in press as: P. Liu, et al., Emerging trends in 2D nanotechnology that are redefining our understanding of "Nanocomposites", Nano Today (2018), https://doi.org/10.1016/j.nantod.2018.04.012

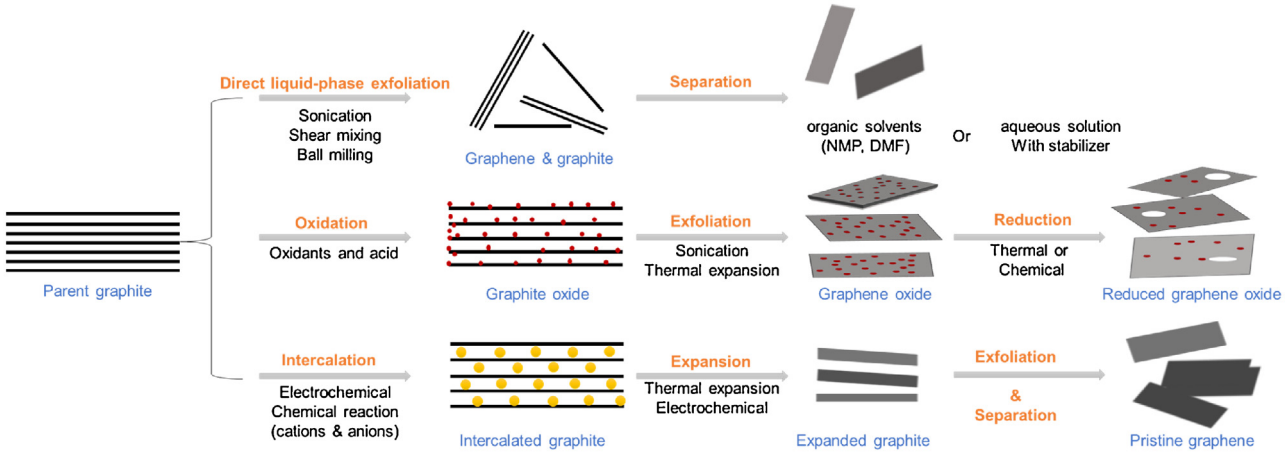

Fig. 5. The production of graphene sheets via a top-down method with graphite as raw materials.

tions as high as 1 mg/mL have been produced. Furthermore, it has been demonstrated that the direct exfoliation methods can be easily scaled up if a proper exfoliation technique is applied (e.g., shear mixing). However, the presence of the dispersant molecules on the nanosheet surface and in the bulk dispersion may be a concern for specific applications of these materials. Moreover, the application of intense and extensive mechanical force to the nanosheets breaks them into smaller pieces; thus, the lateral size of the nanosheets produced via this method barely exceeds 1–1.5 μm.

Covalent functionalization of the nanosheets is an alternative approach that maximizes the exfoliation efficiency and colloidal stability of nanosheets in a dispersion. Production of graphene oxide from parent graphite based on Hummer's method (or the modified versions of the Hummer's method) is the most prominent example of this approach [71,80]. In this method, the parent graphite is intercalated and oxidized in the presence of strong acids and oxidizing agents. This process covalently functionalizes the graphene surface with oxygen-containing groups such as hydroxyl, carboxyl, and epoxide. Eventually, the graphene oxide layers can be easily exfoliated from the graphite oxide via sonication. The most important advantage of this method is its gram-quantity yield, which cannot be achieved using any other top-down or bottom-up methods. Also, the hydrophobicity of the GOx makes it easily dispersible in a range of solvents and simplifies its processing for further applications. The GOx produced using this method often have a lateral size of a few microns and single- to few- layers of nanosheets [81]. However, the oxidation process changes the sp^2 hybridization of the carbon atoms in the basal plane and also introduces some structural and topological defects into the crystalline structure of graphene; thus, the GOx is not electrically conductive [82]. Thermal or chemical reduction of the GOx nanosheets can restore the sp^2-conjugated network and the electrical conductivity to some extent, but complete recovery of the pristine graphene structure in reduced graphene oxide (RGO) is impossible [83].

Electrochemical intercalation and exfoliation is another approach that allows for the production of large, high-quality nanosheets [68,84]. This method uses an electrochemical bias to intercalate nanosheets with various ions. The intercalation process, which can be considered as pre-treatment of the parent material, increases the interlayer spacing while preserving the pristine crystalline structure of the nanosheets. Often, further exfoliation of these intercalated nanosheets via sonication or shear-mixing is required to achieve complete exfoliation [85,86]. However, this exfoliation step can be performed at a lower intensity compared to direct exfoliation methods. Thus, the nanosheets produced by this method have lateral sizes from a few microns up to 50 μm [86]. One drawback of this method is the low colloidal stability of the product; thus, post-processing using dispersant molecules or surface-energy matching solvents is required to assure the colloidal stability in the liquid phase. Electrochemical exfoliation can also produce high-quality thin transition metal chalcogenides (TMCs) such as MoS_2 sheets sizing 5 to 50 μm [87], and 70% of them have 2–5 layers [87]. More information about the electrochemical exfoliation of graphite and other 2D materials can be found in a recent review paper [68].

While the top-down approaches offer high yield and scalability in the production of nanosheets, there are a couple of challenges that need to be overcome before their product can be used unconditionally in any application. The most important issue is the polydispersity of the products of these methods in lateral size and thickness distributions. So far, centrifugation-based techniques have been used to narrow these distributions [88,89]; however, the lateral size and thickness of the nanosheets are coupled properties that have not been accurately disentangled using these techniques. Moreover, only a few tens of milliliters of the dispersions can be processed in each centrifugation cycle, which is a bottle-neck for the large-scale production of these materials [90]. Another issue is the presence of residual or bulk second component (dispersant or solvents) in the final product that is not desired in specific applications, such as electronic devices.

Bottom-up synthesis via chemical vapor deposition

Instead of the "top-down" method using the bulk materials as raw materials above, a "bottom-up" method – chemical vapor deposition (CVD) - can produce large-area, high-quality 2D materials with more structure control [58]. Typically, substrates like SiO_2 or Cu foil can be used to grow 2D sheets such as graphene, TMCs with controlled layer numbers (or thickness), and crystallites (polycrystalline or single-crystalline) in the CVD process. The process is illustrated in (Fig. 6a) with the CVD growth of graphene as an example. The copper foil [91] on a quartz slide or thin nickel film (<300 nm) coated onto SiO_2/Si [92,93] acts as a substrate and methane or other organic vapors such as methanol or ethanol act as the carbon growth source. The growth mechanism of graphene on copper and nickel is different. For the copper substrate, methane will decompose under the catalysis of the copper surface and subsequently deposit onto the surface, nucleate, and polymerize to form graphene (Fig. 6b). For the nickel substrate, carbon atoms will dissolve into the nickel metal at a higher temperature and precipitate out to the surface to form graphene at a reduced temperature. Thin nickel layers with a thickness less than 300 nm is applied

Please cite this article in press as: P. Liu, et al., Emerging trends in 2D nanotechnology that are redefining our understanding of "Nanocomposites", Nano Today (2018), https://doi.org/10.1016/j.nantod.2018.04.012

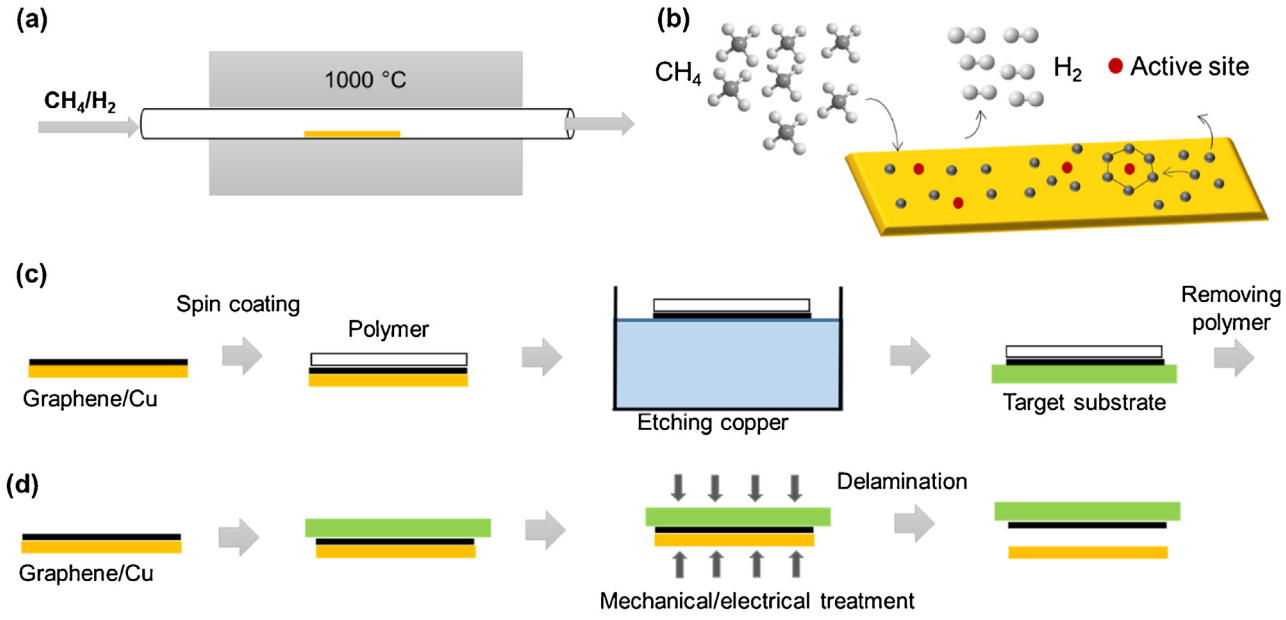

Fig. 6. Chemical vapor deposition of graphene on a copper substrate and its transfer: (a) chemical vapor deposition process; (b) growth mechanism of graphene via deposition; (c) Schematic illustration of the wet transfer process of graphene via etching copper and (d) dry transfer process of graphene via lamination/delamination.

to lower the amount of the dissolved carbon atoms, otherwise thick graphite will form. In these processes, the carbon precursor pressure [94], temperature profile (heating and cooling rate, growth temperature), growth time, substrate types, thickness, surface functionality (e.g., oxygen) [95], and roughness of the metal layer can all affect the graphene growth, its final layered structure, and its performance [96–98]. In addition to graphene, thermal decomposition of transition metal compounds such as ammonium thiomolybdates, molybdenum trioxide [99], and tungsten, under sulfur, selenium, tellurium, and other vapor atmospheres, can produce various transition metal dichalcogenides with controlled size, thickness, composition, and crystallinity [100–102]. The hexagonal boron nitride thin film, few-layers [103–105] or monolayer, [106] and their layered composites with graphene [95,107] can also be produced via CVD technique. In most cases, the atomic thick 2D materials grown by the CVD method need to be transferred from their metal substrate to other support materials for further manipulation and characterization. Two transfer methods, including wet transfer (Fig. 6c) and dry transfer (Fig. 6d), have been used [108].

Wet transfer method: Fig. 6c shows a typical wet transfer process using CVD graphene (CVDG) as an example. A thin supporting layer (SL) is deposited or spin-coated onto CVDG grown on the copper substrate [91,109–112]. The SL is usually a polymer layer, and poly (methyl methacrylate) [109] and polyethylene terephthalate (PET) [113,114] are the most widely used ones due to their ease of manipulation and low cost. Further heat treatment or annealing can soften the polymer layer and improve their attachment with the CVDG. Further etching of the copper substrate with etchants such as sodium/ammonium persulfate [113,115], iron (III) chloride [116,117], and iron (III) nitrate [91] can delaminate the CVDG/polymer film from the copper. Note that the complete etching of the growth substrate is a challenge, and the residual metal particulates can degrade the performance of 2D layers in practical applications. For this reason, extra cleaning technologies are sometimes conducted for their removal [112]. After transfer, PMMA, or another polymer layer, can be dissolved by solvents, such as chlorobenzene, toluene, and acetone, and/or thermally decomposed at 350 °C – 450 °C in a few hours [108], [118]. The types of polymer used have effects on the transfer quality. Polycarbonate [108] and polyisobutylene [119] can be removed easily by organic solvents or even thermal treatment to obtain a clean transfer with fewer polymer residues (which will affect the electronic properties of the 2D layer) and result in few cracks. Thermal released tapes (TRT) are often used as the freestanding supporting layer for the wet transfer process [113,115,120]. This wet-transfer technique is the most widely used method, due to its simplicity and versatility, and the integrity of the 2D sheet after transfer can be well maintained. The disadvantages are that it can be time-consuming, have a high cost (non-reusable growth substrates and waste treatment), and result in contamination -restricting their larger-scale application industrially [108]. New improvements including bubbling [110] and sonication-assisted [121] delamination or direct peeling [120] with water infiltration [122,123] have been reported to address these challenges.

Dry transfer method: In the dry transfer method (Fig. 6d), no steps involve the use of solvents or wet chemical etchants [124–128]. The target substrate first laminates onto the CVD graphene (or other 2D materials) grown on the substrate and then delaminates together with the 2D sheet mechanically. Apparently, the adhesion energy between CVD graphene/target substrate should be higher than that between CVDG/copper for successful transfer. Various treatments such as applying mechanical and electrostatic force, thermal heating in a low vacuum environment [124,128], and creating chemical [124,126] or physical bonding [125] between the 2D sheet and the target substrate have been reported to increase this adhesion energy. Subsequently, the remaining growth substrate, copper in this example, is undamaged and can be reused for further CVD growth. Fewer impurity residues and contaminants are introduced during this process. The reusability of the growth substrate reduces the level of chemical waste, and large-scale transferability of 2D materials [125] using this technique suggests that the dry transfer method is more promising for large-scale industrial applications. Moreover, this process is very compatible with the thermal plastic polymer substrate. However, the delamination step can introduce mechanical defects/cracks/holes on the 2D sheet, and this will need to be overcome in future.

Regarding low-cost mass production of 2D materials, growth at ambient atmospheric conditions and low temperature is important. Although the CVD techniques enable large-area synthesis of

Please cite this article in press as: P. Liu, et al., Emerging trends in 2D nanotechnology that are redefining our understanding of "Nanocomposites", Nano Today (2018), https://doi.org/10.1016/j.nantod.2018.04.012

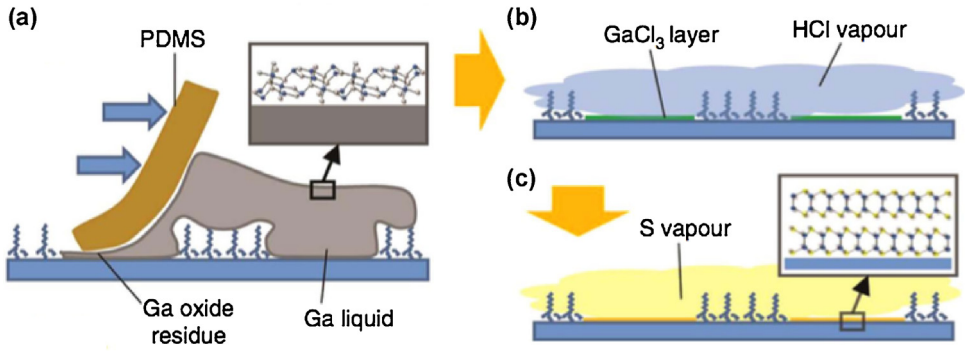

Fig. 7. Fabrication process of screen-printed 2D GaS layers: (a) Liquid Ga is placed on the SiO_2/Si substrate and spread with PDMS, leaving a Ga oxide layer on the upper surface of Ga. (b) HCl vapor treatment transforms the oxide into $GaCl_3$ layer at low temperature (~ 300 °C). (c) Sulfurization by exposure of S vapor (reproduced from ref. [129]).

2D materials, they require relatively high temperature. Besides the liquid-phase exfoliation or CVD methods described above, screen-printing technique of uniform 2D materials has been recently demonstrated [129,130]. This technique utilizes liquid gallium metal spread to an atomically thin layer in the screen-printing manner, which leaves an oxide skin layer on the SiO_2/Si substrate at 60 °C (Fig. 7a). This screen-printing facilitates patterned structures of 2D materials using lithographic techniques. In the middle of the fabrication process, a $GaCl_3$ layer is formed by HCl vapor treatment (Fig. 7b). Finally, sulfurization of the $GaCl_3$ layer under the exposure of S vapor produces 2D GaS (Fig. 7c). This relatively low-temperature process allows the use of flexible polymer substrates for growth.

Dispersion and alignment of 2D sheets in the matrix

Top-down methods inevitably expose brittle 2D nanoflakes to mechanical damage that deteriorates their quality, limiting their application in polymer nanocomposites. As an alternative, the approach can inverse: exfoliated 2D materials can be used as the host materials and a small amount of polymer binders can be introduced to promote the interaction between 2D layers. In the following part, we will review and discuss these aspects in detail.

Processing the exfoliated, large-area 2D nanoflakes

The dispersion and alignment of large-area, high-quality 2D sheets in a polymer or other matrix without compromising their pristine properties are major challenges. For solution-dispersed large-area flakes prepared from top-down methods, these flakes are prone to folding, stacking, wrinkling, aggregating, and crumbling during the traditional processing methods, such as a solution or melt-based mixing. Strong, or even modest shear force, from sonication or vigorous stirring during the mixing or extrusion in the melt mixing, will break the large flakes to small sizes. Other issues such as thermal degradation and feeding difficulty are also challenges necessary to overcome [26–28,31,33]. Additionally, the hydrophobic surface of the nanosheets produced by direct exfoliation methods or electrochemical exfoliation is usually incompatible with most of the polymer matrices. This incompatibility can affect the dispersion of these nanosheets in the polymer matrix, as well as the nanosheet-polymer interfacial interactions. To achieve a homogeneous distribution and a better load transfer at the nanosheets-polymer interface, products with more a hydrophilic surface such as GOx are more desirable. Moreover, the functionalized surface of the nanosheets facilitates their interactions with other molecules and their incorporation into polymer matrix using non-traditional techniques. Several alternative manufacturing methods such as in-situ polymerization via monomer intercalation, layer-by-layer (LbL) assembly, and others may address these challenges (Fig. 8), as described below:

The in-situ polymerization method, which mixes the already-exfoliated 2D materials and reactive monomers in either a solution or emulsion [131], can achieve a random distribution of the 2D layers [132] (more literature here) in the matrix or even an interconnected percolation network of 2D nanosheets with high conductivity [131], but the 2D sheets are not well aligned in the matrix. The use of in-situ intercalation polymerization by impregnating reactive monomers into the expanded graphite [133] or other bulk materials [134] (Fig. 8a) can achieve good alignment of the 2D layers with a high aspect ratio in the polymer matrix. If a large size, highly ordered pyrolytic graphite (HOPG) is used, the intercalation polymerization in the expanded HOPG can generate layered nanocomposites with graphene layers that are continuous at the in-plane direction of the composite body [43]. The major challenge of this method is that the thermal expansion of graphite is not complete and often, the expanded structure consists of graphite layers with thicknesses of up to tens of nanometers [134].

LBL assembly is a step-wise method of sequential adsorption/deposition with the dispersed 2D materials, such as a graphene oxide suspension, and the complementary polymer materials via dipping [135], spinning [136], or spraying (Fig. 8b) [135,137]. Layered 2D nanocomposite films or membranes with highly ordered structure and a uniform alignment of the 2D sheets in the plane are possible [138]. The layer chemistry, thickness, and morphology [139] can be precisely controlled, and the alternating layers can bind to each other through electrostatic interactions [135,137], hydrogen bonding [139], or van der Waals forces, providing a diversity of structural designs and control capabilities [138]. The multilayer composite film with aligned GO nanoflakes shows a significant improvement in mechanical strength. For example, the layered GO/poly(vinyl alcohol) film at 1.8 vol% graphene shows a modulus 10 times higher and a tensile strength 250% of the pure poly(vinyl alcohol) samples [138]. Note that the graphene oxides used in that study only have small average sizes of 1 – 2 μm and a thickness of ~0.8 nm (aspect ratio ~ 2000), and a higher mechanical reinforcement is anticipated for GOx fillers with a higher aspect ratio. LBL is suitable for the production of thin composite nanofilms [140].

To accelerate the assembly process of the layered nanocomposites with 2D materials, a continuous technique – vacuum-assisted filtration - can assemble the 2D nanoflakes like graphene oxides [141,142] at the interface between the solution and filter to form graphene nanocomposite papers. The 2D nanosheets, instead of a role of nanoinclusions, behaves as the major component to form layered graphene papers with high strength and conductiv-

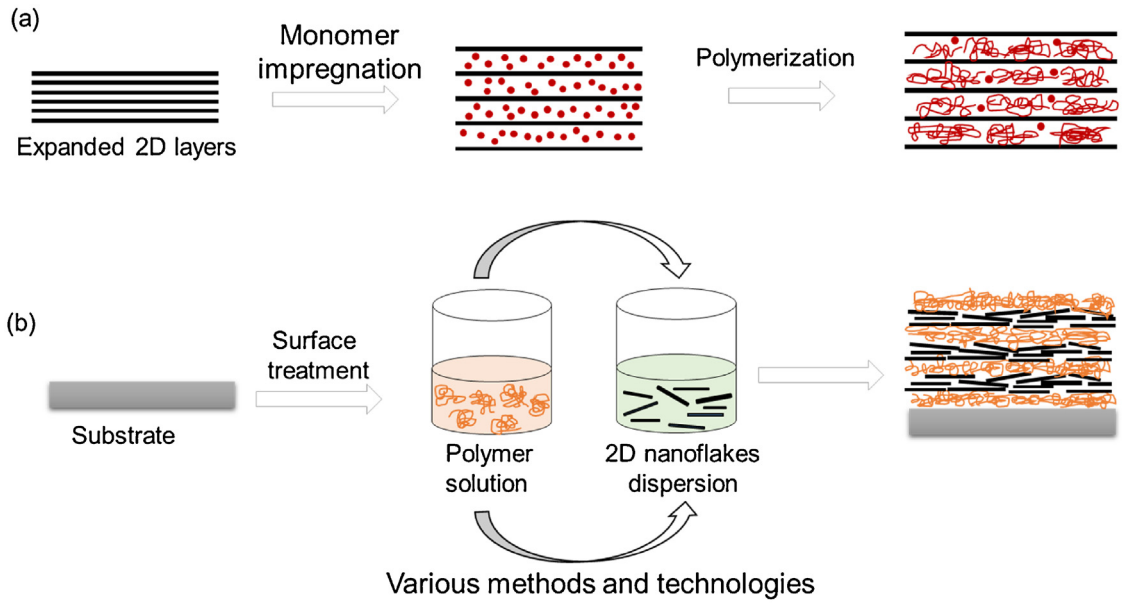

Fig. 8. Fabrication of multilayer nanocomposites with aligned 2D nanoflakes via (a) In-situ intercalation polymerization; (b) Layer-by-layer assembly.

ity [141,143]. A small amount of polymers, organic components, or nanoparticles, 5 vol% for example, is added in the process to bind these nanosheets together either via noncovalent hydrogen/ionic bonding, π–π interactions, or Van der Waals' forces such as hydrophobic interaction, or covalent bonding directly via chemical reaction or a combination of these aspects [144]. This is very similar to the soft protein binders in the nacre structures of nature. In addition, a slow evaporation of the solvent and a continuous precipitation of 2D nanoflakes, such as graphene oxides with binders, can also result in nacre-like structures [145]. Freeze casting (or ice-templating) [146] and other methods have been developed to produce nanocompsosites with layered structures. Nanocomposites with high stiffnesses of tens of GPas and high fracture strengths of hundreds of MPa or even higher have been developed in this way. Here we will not discuss these in detail and readers can refer to several recent review papers to learn more [144].

The exfoliated 2D nanosheets can also be used to produce fibers with aligned layer structure along the longitudinal direction via wet-spinning, dry-spinning, or other methods continuously [147–149]. Exotic graphene fibers with high thermal conductivity of 1290 ± 53 W m^{-1} K^{-1} after graphitization at a high temperature of 2850 °C [150], recoded stiffness of 282 GPa, strength of 1.45 GPa, and an electrical conductivity of 8×10^3 S/cm after graphitization at 3000 °C [151] have been produced. Large-area monolayer graphene oxide nanosheets with an average width of ≈ 23–24 μm and an aspect ratio of 2.6×10^4 have been used in the studies [151]. Obviously, the alignment of the 2D materials to form a highly ordered hierarchical structure at a high volume fraction promises the development of lightweight/high strength nanocomposite materials with multiple functions in the future. It will be quite interesting to see the mechanical robustness and more exotic functions we can achieve in the future for the composites using 2D nanomaterials with higher aspect ratio.

Processing large-area 2D materials grown by CVD method

The long-range continuousness and controlled layer thickness of 2D materials grown by CVD method provide a new opportunity to test the theoretical limit of reinforcement in nanocomposites with semi-infinite nanoinclusions. The resulting nanocomposites can be highly anisotropic with the maximum reinforcement at the direction parallel to the 2D sheets. Because these 2D materials have been grown on or transferred to a certain substrate with an arbitrary size, their dispersion into matrix materials, such as polymers or metals, can be carried out in a controlled way using the layer of substrate/2D sheets as a building block. Processing techniques such as stacking/laminating, folding, rolling, hot-pressing, and others can assemble these thin films into planar-layered composites or fibers [43,152,153] and others with alternating 2D layer and matrix layer. This is a modular way characterized by a precise control of the dispersion of the 2D sheets in the matrix materials [154]. The aggregation and the damage of the large-area 2D sheets are also avoided to the greatest extent. Moreover, the continuous 2D inclusion can span the physical dimensions of the matrix and results in percolation with only a single layer at an atomic thickness, which can yield nanocomposites with the maximum mechanical and functional reinforcement, as predicted by those equations in the section above.

Specifically, an early study from the Skákalová group found that the use of few-layer graphene grown by the CVD method with nickel substrate to cover PC film, can reinforce Young's modulus (E) of pristine polycarbonate (10 μm thick) from 1.37 GPa to 1.85 GPa, and the apparent E value of the FLG is 4.6 TPa [155] and the sheet resistance is 800 Ω/sq. When compositing continuous monolayer graphene into a metal matrix to form layered nanocomposites consisting of alternating layers of monolayer graphene and copper (70 nm thick) or nickel (100 nm thick) (Fig. 9a), graphene with high intrinsic mechanical strength can block dislocation propagation across the metal-graphene interface and strengthen the composite by 31–52% when compared with the pure metal matrix [156]. The Lambin group demonstrated that multilayered (1–4 layers) composites generated by stacking PMMA/graphene film (Fig. 9b) could be used as an efficient optically transparent and flexible shielding media of electromagnetic fields [152]. Vlassiouk and coworkers [153] have reported the continuous stacking of 16 layers of Gr/PMMA films to form $(Gr/PMMA)_{16}$ laminate nanocomposites with a PMMA layer thickness of 250 nm. They also reported the rolling of PMMA film with 1 or 6 layers of graphene to generate Gr_1/PMMA and Gr_6/PMMA fibers using a wire-guided method [157] (Fig. 9c).

The graphene, with a volume fraction of 0.13%, almost doubled E and increased the strength (σ) by 25%, when comparing the lam-

Please cite this article in press as: P. Liu, et al., Emerging trends in 2D nanotechnology that are redefining our understanding of "Nanocomposites", Nano Today (2018), https://doi.org/10.1016/j.nantod.2018.04.012

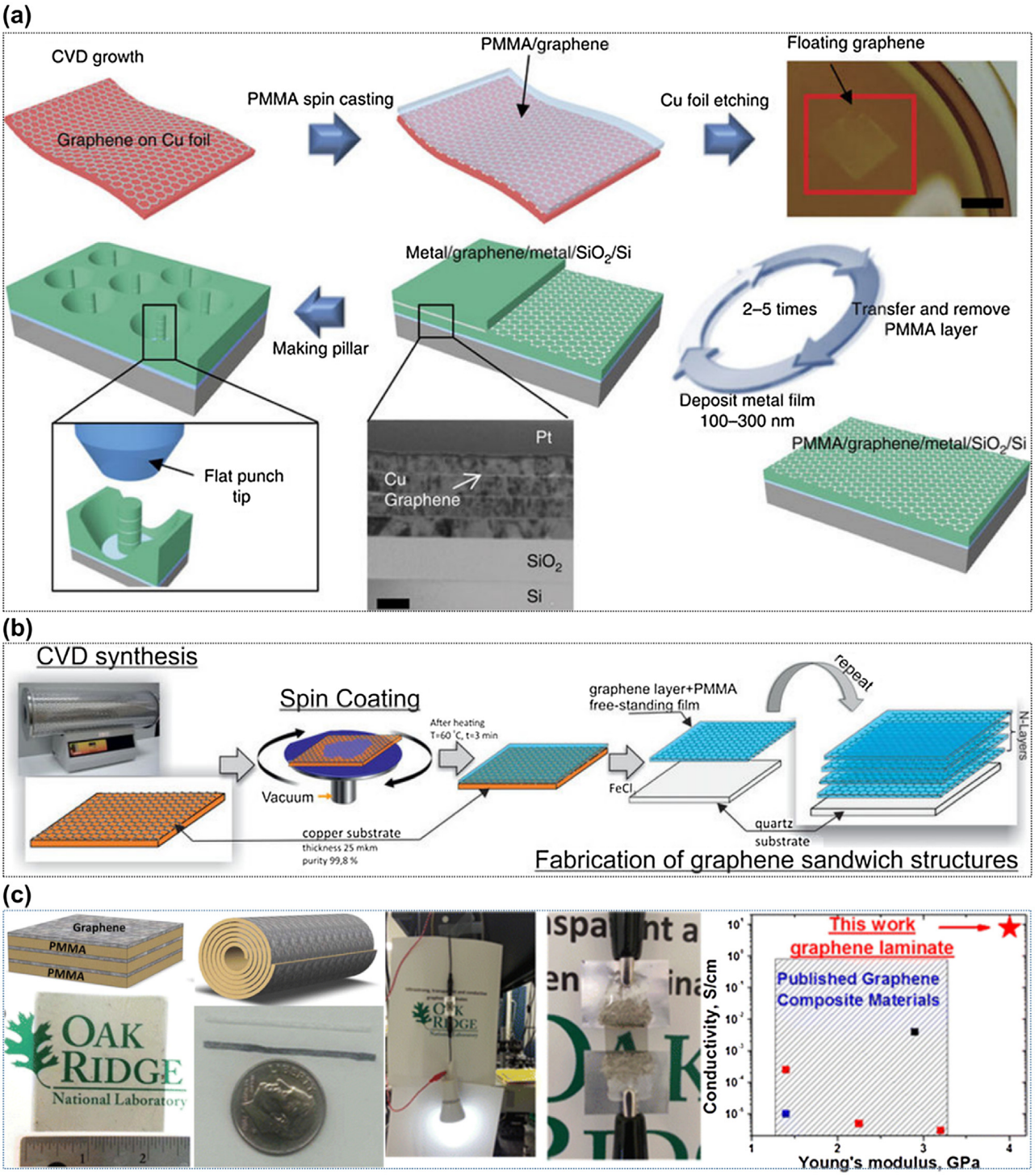

Fig. 9. Various nanocomposites with CVD graphene: (a) layered metal (copper or nickel)/graphene nanocomposites with improved strength, reproduced with permission from [156]. Copyright (2013) Springer Nature. (b) Layered graphene/PMMA nanocompsoites for an efficient electromagnetic field absorption, reprinted (adapted) with permission from [152]. Copyright (2014) Springer Nature. (c) Graphene-based composite fibers and laminates with high stiffness and electrical conductivity reprinted (adapted) with permission from [153]. Copyright (2015) American Chemical Society.

inate composite with the neat PMMA, and the effective E and σ of graphene were determined to be 11 ± 6.7 GPa and 1.2 ± 0.5 TPa, respectively. The hollow fibers demonstrated similar enhancement with an efficient graphene strength of 19 ± 9 GPa. When washing away PMMA from the Gr_6/PMMA fiber, leaving only $(Gr)_6$, the graphene fiber shows a modulus of up to 0.3 TPa and a strength of 2.2–4 GPa. These values are higher than most of those reported for CNTs and graphene yarns and are competitive with carbon fibers. These composites are also highly conductive with an amount of 8.1 S/cm at only 0.13% graphene [153], and the pure graphene fibers have a conductivity of 5×10^3 S/cm, on the same order as graphene fibers based on the exfoliated graphene above [151].

The results above promise the development of lightweight, high strength, and multifunctional nanocomposites or their fibers by using graphene or other 2D materials grown by the CVD method. One of the biggest challenges, however, is how to scale up the man-

Please cite this article in press as: P. Liu, et al., Emerging trends in 2D nanotechnology that are redefining our understanding of "Nanocomposites", Nano Today (2018), https://doi.org/10.1016/j.nantod.2018.04.012

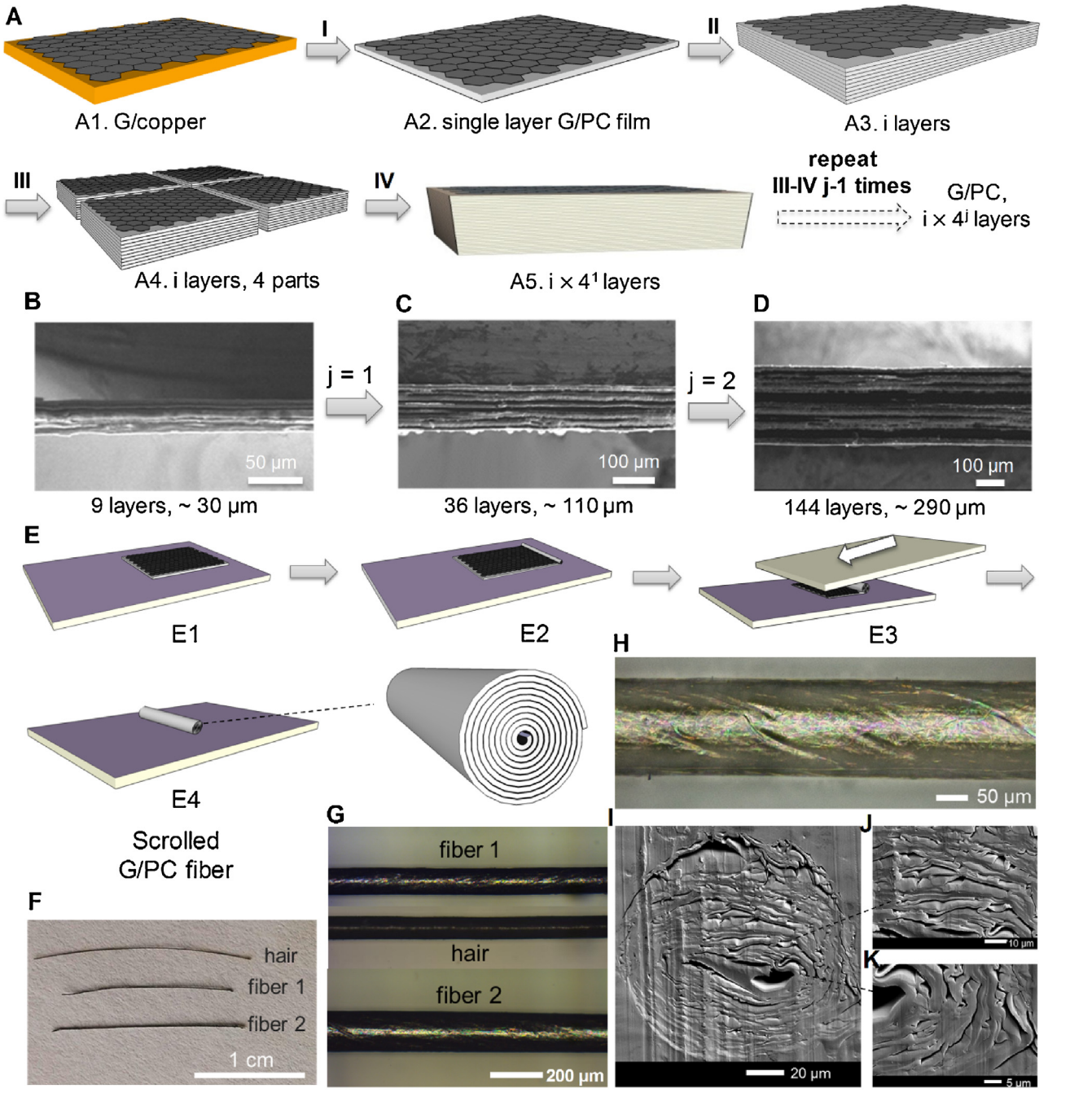

Fig. 10. Fabrication of graphene/polycarbonate (G/PC) composites with aligned, semi-infinite CVD graphene: (A) 4^j stacking method for planar 4^j composites: (I) spin-coating and etching, (II) stacking, (III) cutting/folding, and (IV) stacking and hot-pressing. (B)-(D) are scanning electron microscope (SEM) images of the planar composites with i = 9 (3570 nm/layer, $V_G \approx 0.009\%$), j = 1, and 2, respectively. (E) The transverse shear method for scrolled nanocomposite fiber: (E1) a single layer of G/PC film on Si/SiO_2 substrate, (E2) the film with folds at one end created by a glass capillary, (E3) the scrolling of the film by the transverse shear force exerted by the two Si/SiO_2 wafers, and (E4) a scrolled fiber with Archimedean spiral pattern in the cross-section plane. (F–I) The optical microscope image of fiber 2 with $d = 160 \pm 4$ μm and fiber 1 with $d = d = 131 \pm 3$ μm. (J)-(L) are SEM images of fiber 2 in the cross-section plane, scaling bars are 20, 10, and 5 μm, respectively. Reproduced (adapted) with permission from [43]. Copyright (2016) American Association for the Advancement of Science.

ufacturing process starting from thin layers of 2D materials with nanometer thickness to a macroscopic-scale product [158]. The scalability is a critical bottleneck in the research of nanomaterials and one must to overcome to make a tangible impact in the real world [25]. Recently, our group has reported a 4^j folding/stacking method to scale up the production of layered nanocomposites with aligned CVD graphene [43]. The whole process, as illustrated in Fig. 10. Graphene layers will replicate and increase exponentially as 4^j after each folding and stacking, rapidly scale from a few layers to hundreds of layers (i.e., 320 layers) and the sample thickness increases from nanometer scale to sub-mm scale (Fig. 10a–d). In this process, the sample will copy their layer structure and composition during each folding/stacking and the final layered composite will have the exact same structure as the beginning. Large-area 2D materials like those 30-inch CVD graphene film [159] or 100-m-long CVD graphene [160] produced via roll-to-roll growth and transfer method will bring this process more practical significance. In addition, our group has also reported a new transverse shear scrolling method to conveniently produce scrolled fiber with well identified Archimedean spiral patter [43] (Fig. 10e–k) starting from

Please cite this article in press as: P. Liu, et al., Emerging trends in 2D nanotechnology that are redefining our understanding of "Nanocomposites", Nano Today (2018), https://doi.org/10.1016/j.nantod.2018.04.012

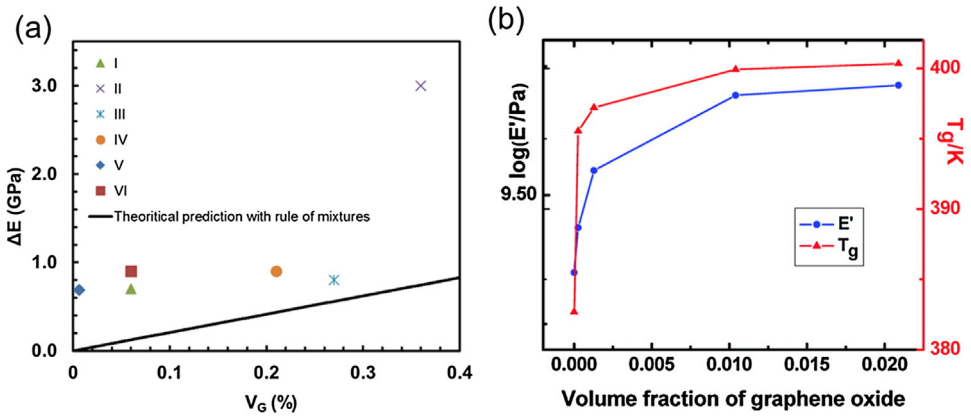

Fig. 11. (a) Plot of various ΔE data against V_G, data points I-IV from Literature sources. The theoretical prediction curve is based on the rule of mixtures with the efficient modulus of monolayer GOx = 207.6 GPa determined by AFM [170]. Reproduced with permission from [43]. Copyright (2016) AAAS. (b) Glass transition temperature and storage tensile modulus E′ of PMMA/graphene oxide at 313 K versus graphene oxide loading. Reproduced with permission from [171]. Copyright (2012) American Chemical Society.

a single layer of graphene/PC film, this technique also scale the nanocomposite from nanometer-thick thin film to a microfiber. These nanocomposites also show significant mechanical reinforcements at a graphene volume fraction of 0.082%, and the planar composites have anisotropic electrical conduction even at 0.003% [43].

Reinforcing performance and applications

Mechanical reinforcement and applications

In the 4^j stacking CVDG/PC layered nanocomposites, a linear enhancement of the elastic modulus in the longitudinal direction with respect to V_G is observed - about 1.0 GPa at V_G of 0.185% with an efficient graphene modulus of 500 GPa - which is similar to those reported values of CVD monolayers [161,162], approaching the limit of platelet filler theory – rule of mixtures. Interestingly, the glass transition temperature (T_g) of the composite is even lower than the polymer matrix (i.e., 141.8 °C *vs.* 147.7 °C). A similar finding has also been reported for laminated nanocomposites of CVDG/PMMA: the T_g of $(Gr/PMMA)_{16}$ laminates is 3 °C lower than that of pure $(PMMA)_{16}$ (250 nm per layer) [153]. These results are contrary to several reported nanocomposites with GOx or their derivatives [26–28,31,33], wherein the polymer matrix such as PVAs or PMMAs can bind well with the GOx nanoplatelets [163–169]. Under such conditions, adding a very small amount (e.g., less than 0.5 vol%) of GOx can also significantly reinforce the mechanical properties, such as the stiffness of the matrix materials (Fig. 11a). Such an enhancement is even higher than the theoretical limit predicted by the rule of mixtures using E_{GOx} = 207.6 GPa [170] (Fig. 11a). Such a reinforcement, however, may not linearly scale into a higher filler content, and the further addition of nanofillers may even compromise the achieved reinforcement [122–128].

An early study from Droste and Dibenedetto in 1969 explains the above results. Changes or reinforcement in the physical properties of the composites can separate into two contributions - one caused by the matrix undergoing modifications and the other is related to mechanical reinforcement by the filler particles [172]. The increase of the glass transition temperature for nanocomposites with GOx or their derivatives [26,163] indicates a reduced chain mobility of the polymer molecules due to strong interactions with, or binding to, nanofillers at the interface [170,171]. This contribution is from a matrix modification and appears to be a major reason for the reinforcement in GO nanocomposites (Fig. 11b). To separate the influence of thermoviscoelasticity, Hashin's viscoelastic micromechanics can be considered, and $\frac{E_c(T-T_g)}{E_m(T-T_g)} - 1$ can be used to calculate the corrected mechanical reinforcement by nanofillers, instead of $\frac{E_c(T)}{E_m(T)} - 1$ [170,171].

Alternatively, the stiffness reinforcement in the layered and scrolled composite systems with the reduced glass transition temperatures should come from load transfer to the continuous graphene sheets directly. There exists a direct stress transfer from the polymer matrix layer to the graphene layer in these composites, considering the graphene size is much larger (10 times) than the critical size – 30 microns, as mentioned above [43,157]. It would be quite interesting to see if the reinforcement in these layered and scrolled composites can further scale up at a higher CVDG content. For example, a modulus enhancement of 20.6 GPa at V_G of 2.5% in the longitudinal direction is anticipated [43]. With such high reinforcement, the composite materials can be used as armor materials for protection applications, according to theoretical calculation results from Wetzel group and our group [173,174]. The in-plane mechanical isotropy of the graphene filler can provide distinct advantages when use the nanocomposites are used as barrier materials [174]. However, at high volume fraction of graphene, fabrication becomes a significant challenge. For example, V_G of 2.5% corresponds to a polymer layer thickness of 13.3 nm when monolayer graphene is used as the inclusion. Robust, interfacial bonding between the polymer layer and graphene layer is also necessary, considering that a shear sliding between the pristine graphene layer and the polymer layer (e.g., PMMA or PET) will occur at a critical strain about 0.4% [35,175]. Otherwise, the low shear strength of the layered composites cannot be used as stand-alone structural materials; rather they would be best suited as solid lubricants, such as graphite.

Besides the similar stiffness reinforcement [43,153], the scrolled fibers with the continuous 2D graphene layer completely spanning the physical dimension of the composite body also show unique mechanical deformation and fracture behavior during the tension test [43]. Telescoping/twisting between layers occurs during elongation because of the relatively weak interlayer binding, while the elongation of each polymer layer can lead to a transverse contraction in the radial direction, which depends on the Poisson' ratio of the polymer layer (Fig. 12a). This contraction, however, will yield a compression force between the layers, increase the friction force between the layers, and prevent the telescoping and sliding between the layers. Therefore, we can find a "stick-slip" pattern of the scrolled fiber during the tensile test, as evidenced by the

Please cite this article in press as: P. Liu, et al., Emerging trends in 2D nanotechnology that are redefining our understanding of "Nanocomposites", Nano Today (2018), https://doi.org/10.1016/j.nantod.2018.04.012

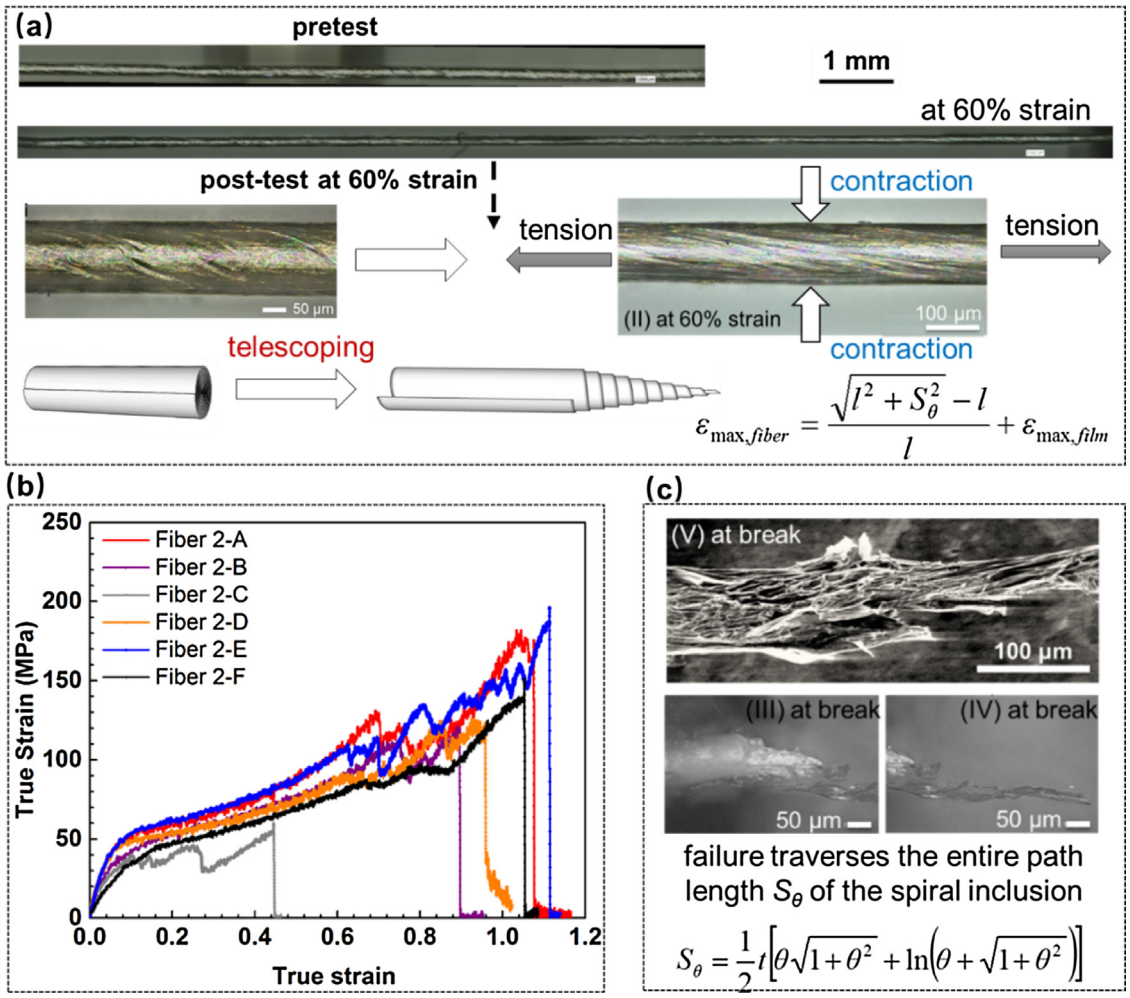

Fig. 12. The mechanical deformation and elongation of a scrolled CVDG/PC fiber. (a) Telescoping/twisting behavior of the fiber during the longitudinal tension, (b) SEM images of the fracture behavior of scrolled fiber, and (c) tensile curve of the scrolled fiber with V_G = 0.082%. Reproduced (adapted) with permission from [43]. Copyright (2016) American Association for the Advancement of Science.

fluctuated tensile curves in Fig. 12b. The fracture of the scrolled fiber proceeds in a way such that the failure traverses the entire path length of the spiral 2D films (Fig. 12c), and thus, the rupture of the graphene inclusion may take place over a large strain. This is very different from traditional carbon fibers or Kevlar fibers with a relatively homogeneous cross-section, where the breakage occurs instantaneously and catastrophically. Such a unique fracture behavior may explain why we can still achieve a strength enhancement = 40 MPa of the composite fiber at a higher elongation > 100% of true strain at V_G = 0.185% with an effective graphene strength of about 21.6 GPa. A further study of this deformation mechanism of the scrolled fiber (e.g., using *in-situ* Raman mapping) [176], could be beneficial to obtain a quantitative understanding of the deformation mechanism and the role of graphene in the reinforcement.

Finally, we would like to conduct a comparison the above nanocomposites with those widely used carbon fiber composites with superb mechanical performance in the market. The carbon fibers have a typical elastic modulus of 200–300 GPa, an elongation at break of 1-2%, and an ultimate strength about 4 GPa, while 2D sheet like graphene has much a higher elastic modulus of 1000 GPa, elongation of 0.25∼0.3, and fracture strength of 125 GPa. Although these results are tested by AFM at a microscale, it does show the possibility that 2D layered composites could have higher strain energy density [173,174] and mechanical performance than carbon fiber composites at a same amount of the fillers. Therefore, 2D layered composites provide a new opportunity for the development of ultra-lightweight and super strong materials in the future. In addition, due to its in-plane isotropicity, 2D membrane or layered composite has a tensile wave speed $\sqrt{E/\rho}$, E is the elastic modulus, and ρ is the density) and thus a critical penetration velocity approximately $\sqrt{2}$ times that of the traditional woven fabric with identical mass and tensile properties (see ref. [177] for details). Therefore, the 2D layered composite has its unique advantage in the applications as protection materials, e.g., body armor and ambient armor [173,174].

Barrier performance and applications

As discussed in the theoretical section, the use of large-area, high-quality 2D materials, such as graphene, can minimize the required amount of nanomaterials to achieve a good barrier performance. There are works from several different groups reporting the use of monolayer or multilayer CVD graphene as a surface barrier layer to significantly reduce water vapor transmission rate (WVTR), to protect organic electronics [178,179] or prevent the water-induced corrosion [180]. Specifically, Choi et al. have found that the WVTR value of 6-layer graphene on PET films was about 10^{-4} g/m^2·day during the first few hours and gradually increased to 0.48 g/m^2·day. This value, however, remains 7 times lower than bare PET films. The graphene-passivated organic field-effect transistors exhibit excellent environmental stability

Please cite this article in press as: P. Liu, et al., Emerging trends in 2D nanotechnology that are redefining our understanding of "Nanocomposites", Nano Today (2018), https://doi.org/10.1016/j.nantod.2018.04.012

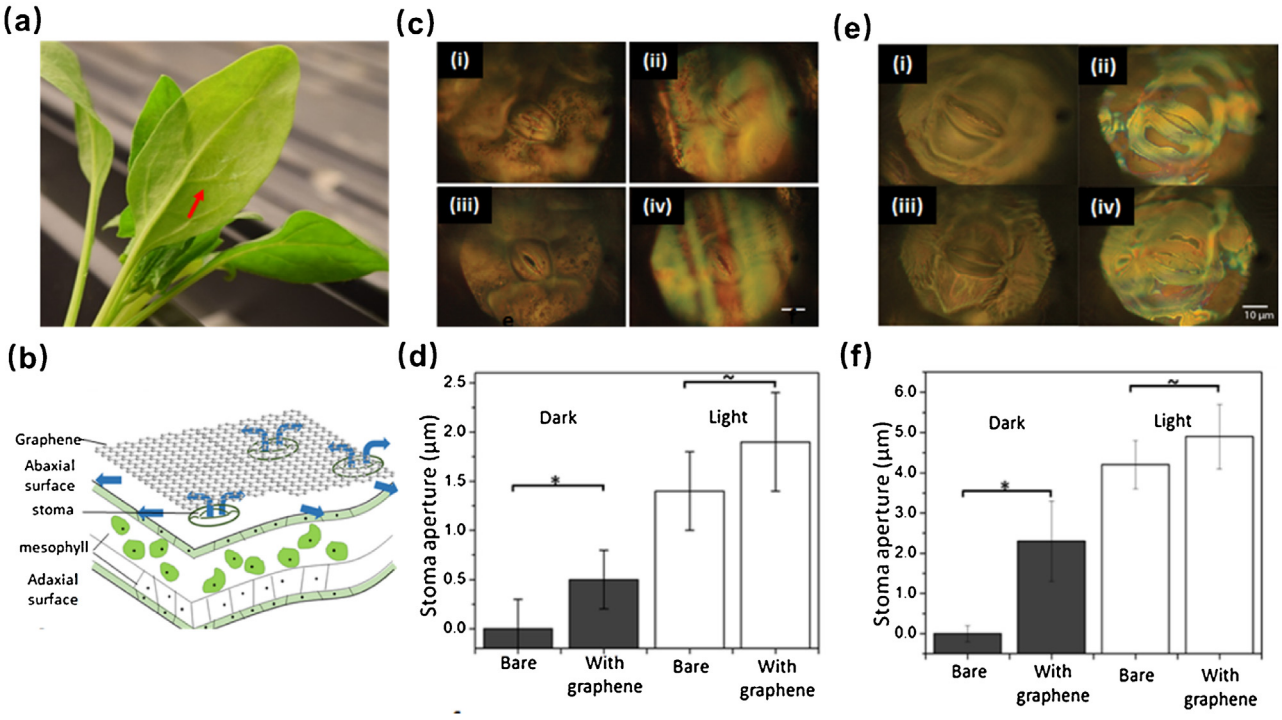

Fig. 13. Graphene-PMMA-Peace lily hybrid. (**a**). A graphene leaf hybrid material can regulate analyte residence time within the leaf while maintaining stomatal activity. **(b).** Graphene-PMMA is deposited on the abaxial surface of a spinach (*Spinacia Oleracea*) leaf. (**c**). (i)-(ii) The stomata of a spinach plant are shown with and without graphene-PMMA deposited on the leaf surface both in the dark and, (iii)-(iv) when plants were exposed to 10 mW/cm^2 white light lamp (Sinostar, FL-70W) for 2 h. (**d**). Stomatal aperture of the spinach plant is monitored with graphene-PMMA and without (control) in the dark (unpaired t-test, $p < 0.05$) and after exposure to white light (unpaired t-test, $p > 0.05$, i.e., no statistical difference). Error bars are standard deviations ($n = 5$). (**e**) (i)-(ii) The stomata of a peace lily plant are shown with and without graphene-PMMA deposited on the leaf surface both in the dark and, (iii)-(iv) when plants were exposed to 10 mW/cm^2 white light lamp (Sinostar, FL-70W) for 2 h. (**f**) Stomatal aperture of the peace lily plant is monitored with graphene-PMMA or without (control) in the dark (unpaired t-test, $p < 0.05$) and after exposure to white light (unpaired t-test, $p > 0.05$, i.e., no statistical difference). Error bars are standard deviations ($n = 5$). Reproduced (adapted) with permission from [181]. Copyright (2016) Springer Nature.

and a prolonged lifetime even after 500 bending cycles [178,179]. Seethamraju et al. later demonstrated a WVTR as low as 10^{-6} g m^{-2} day^{-1} for large-area CVD monolayer graphene-embedded polymers (GEPs) and the use of these GEPs as excellent encapsulating materials for organic photovoltaic (OPV) devices [178,179]. Wang et al. have studied the anticorrosion performance and mechanism of the single- and double-layer graphene-coated glasses in water for 120 days, and found that the glass experienced negligible changes in both fracture strength and surface roughness, compared with a significant increase in surface roughness and defects and reduction in fracture strength of the unprotected glass [180].

Recently, another interesting application of the barrier properties of large-area CVDG is on the interface of such materials with plants. Our group has demonstrated that grafting a thin CVDG/PMMA composite film onto a leaf can aid in the regulation of stomatal behavior (Fig. 13) [181]. Further interfacing of nanomaterials with plants has also led to some early discoveries in opportunities to augment plant functions, such as enhanced photosynthesis [182]. Such technologies typically depend on exploiting the high stability and unique chemical and physical traits of nanomaterials. For instance, graphene derivatives single-walled nanotubes (SWNTs) embedded within chloroplasts have the potential to enhance the light reactions of photosynthesis with their distinctive optical and electronic properties [182]. SWNTs absorb light over a broad range of wavelengths in the ultraviolet, visible, and near-infrared spectra not captured by the chloroplast antenna pigments, which potentially allows the plant to utilize a broader spectrum of wavelengths for photosynthetic activity.

Electrical properties and applications

Capacitors

As mentioned above, the layered composite with CVD graphene has demonstrated an anisotropic conduction with high electrical conductivity in the plane while being insulated across the plane, even at V_G 0.003% [43]. Actually, the continuous CVD graphene sheet with low-sheet resistance can be used as a thin electrode or circuit layer, either covered on the surface or embedded into the matrix of specific materials in order to provide a capability of electrical conduction parallel to the 2D sheet (e.g., transparent electrodes for touch-screen panel) [159]. The further control of the dispersion/distribution of the conductive layers inside the matrix materials can render a composite body with more advanced functions, electromagnetic shielding media [152] and capacitors [183] with multilayer structure configuration, for example (Fig. 14a).

Inductors

The Archimedean scroll geometry of the aforementioned 2D composite scrolls also forms the basis of many fundamental electrical components, most notably, spiral inductors (Fig. 14b). An inductor is a passive two-terminal electrical component that stores electrical energy in a magnetic field when an electric current is flowing through it. An inductor typically consists of an electric conductor, such as a wire, that is wound into a coil. Along with capacitors and resistors, inductors are one of the three passive linear circuit elements that make up electronic circuits. Inductors are widely used in alternating current (AC) electronic equipment, particularly in radio equipment. They are used in electronic filters to separate signals of different frequencies, and in combination

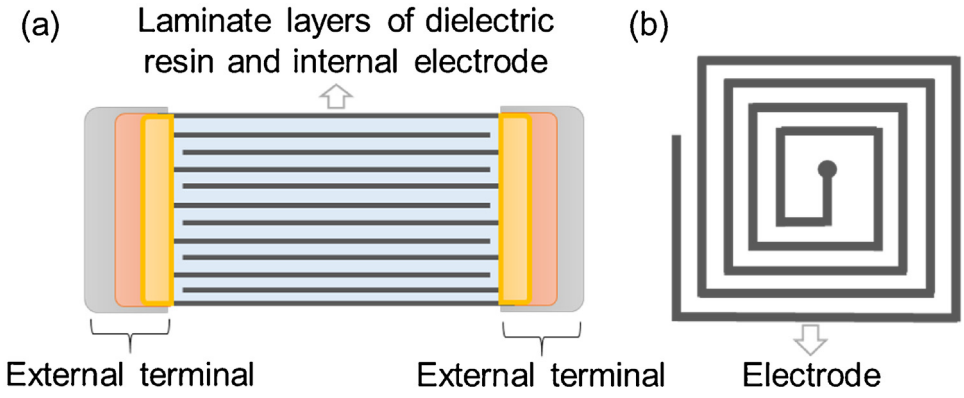

Fig. 14. (a) Capacitor and (b) spiral inductor with 2D graphene inclusion at a multilayered and scrolled configuration.

with capacitors to make tuned circuits, used to tune radio and TV receivers.

Inductors come in many shapes. Most are constructed in enamel coated wire (magnet wire) wrapped around a ferrite bobbin with wire exposed on the outside, while some enclose the wire completely in ferrite and are referred to as shielded. Small inductors can be etched directly onto a printed circuit board by laying out the trace in a spiral pattern. Some such planar inductors use a planar core. The miniaturization of the 2D planar coils is typically achieved with metal deposition along with lithographic techniques [184–188]. Inductors fabricated as such have found many applications such as radio frequency (RF) signal transmission, power electronics, and wireless sensors [189–191].

In order to cope with the parasitic energy losses at high frequency for all of these applications, a lot of these planar inductors does not use ferromagnetic cores. Air core coils have lower inductance than ferromagnetic core coils but are often used at high frequencies because they are free from energy losses - called core losses - that occur in ferromagnetic cores, which increase with frequency. At high frequencies, particularly radio frequencies (RF), inductors have higher resistance and other losses. In RF inductors, these losses are typically due to skin and proximity effects. Radiofrequency alternating current does not penetrate far into the body of a conductor but travels along its surface. Therefore, in a solid wire, most of the cross-sectional area of the wire is not used to conduct the current, which is in a narrow annulus on the surface. Proximity effect, on the other hand, occurs in parallel wires that lie close to each other. The individual magnetic field of adjacent turns induces eddy currents in the wire of the coil, which causes the current in the conductor to be concentrated in a thin strip on the side near the adjacent wire. Like the skin effect, this reduces the effective cross-sectional area of the wire conducting current, increasing its resistance. It is interesting to note, that atomically thin 2D materials are ideal candidates for patterning such planar inductor circuits to reduce the local concentration of electrical currents. 2D materials are basically the extreme analogs of "Litz wires", which divide an otherwise thick wire into some thinner strands to evenly distribute the current density, resulting in a larger cross-sectional conduction area than an equivalent single wire, therefore reducing skin effect losses.

Efforts are extending the planar geometry of such microscale inductors into the third dimension via mesostructures, most notably through techniques such as "compressive buckling" that assembles planar micro/nanomaterials into complex 3D architectures, have been reported [192,193]. This illustrates that the strain relaxation in an elastomeric substrate simultaneously imparts forces at a collection of lithographically controlled locations on the surfaces of planar precursor structures. A 3D spiral inductor for near-field communication has been constructed following this strategy, highlighting enhanced quality factors and broader working angles compared to those of conventional 2D counterparts [193]. We note, however, that this mechanically tunable inductor device is still constructed with conventional bulk materials (9 μm copper/12 μm polyimide bilayers, with 1 μm SiO_2 encapsulation). This, once again, underscores the immense potential of the 3D architecture brought forth by geometry such as the Archimedean scrolls made using 2D material composites in realizing these highly complex capabilities.

It is well known in traditional spiral inductor fabrication (Fig. 14b), that in the limit of low radial operating frequencies ω, increasing the number of turns N improves the quality factor ($Q = \omega L/R$) because the inductance L scales as N^2 while the inductor resistance R varies linearly with N. Similarly, increasing the radius r of an inductor improves Q because L varies as r^2 while R varies linearly with r. So high Q air core inductors often have large diameters and many turns, again highlighting the advantages of scalable fabrication techniques of 2D material composite scroll fibers. In addition, inductors are not restricted to air core, in traditional fluxgates. For example, permalloy and Co-based amorphous alloys are used as magnetic core materials [194]. Over the years, researchers have experimented with growing the core during the fabrication process, such as sputtered [195] and electrodeposited permalloy [196–198] and amorphous ferromagnetic Co-P alloy [199] as core materials in microsensors. Incorporating magnetic cores in geometries such as the Archimedean scrolls, however, could potentially be a straightforward task [153,157]. One can imagine integrating the core materials within the center of these 2D composites or even into the composite itself, depending on the applications.

Particle state machines

Cubic millimeter-sized devices, called "smart dust", are the smallest dispersed electronic devices reported to date [200]. While the initial concept was developed more than 15 years ago, further progress was hindered by the lack of efficient energy storage technologies. Indeed, light-weight batteries do not provide enough power, often forcing small robots to rely on external energy harvesting. To this end, some versions of smart dust harvested energy from wireless electromagnetic radiation, limiting the devices' operation to a distance of a few meters [200]. Unfortunately, this approach cannot be scaled down, due to receiver size limitations [201]. Alternative energy harvesting techniques (chemical power harvesting [202], bacteria-produced power [203], ultrasound [200], magnetic field [204], and light [205]) are continuously being developed, delivering microwatts of power on the micrometer scale but, so far, have had little to no success in powering energy-thirsty electronics (usually requiring milliwatts). The issue of energy deficiencies can be circumvented using novel 2D devices that require only microwatts, or even nanowatts, of power. Built from 2D mate-

Please cite this article in press as: P. Liu, et al., Emerging trends in 2D nanotechnology that are redefining our understanding of "Nanocomposites", Nano Today (2018), https://doi.org/10.1016/j.nantod.2018.04.012

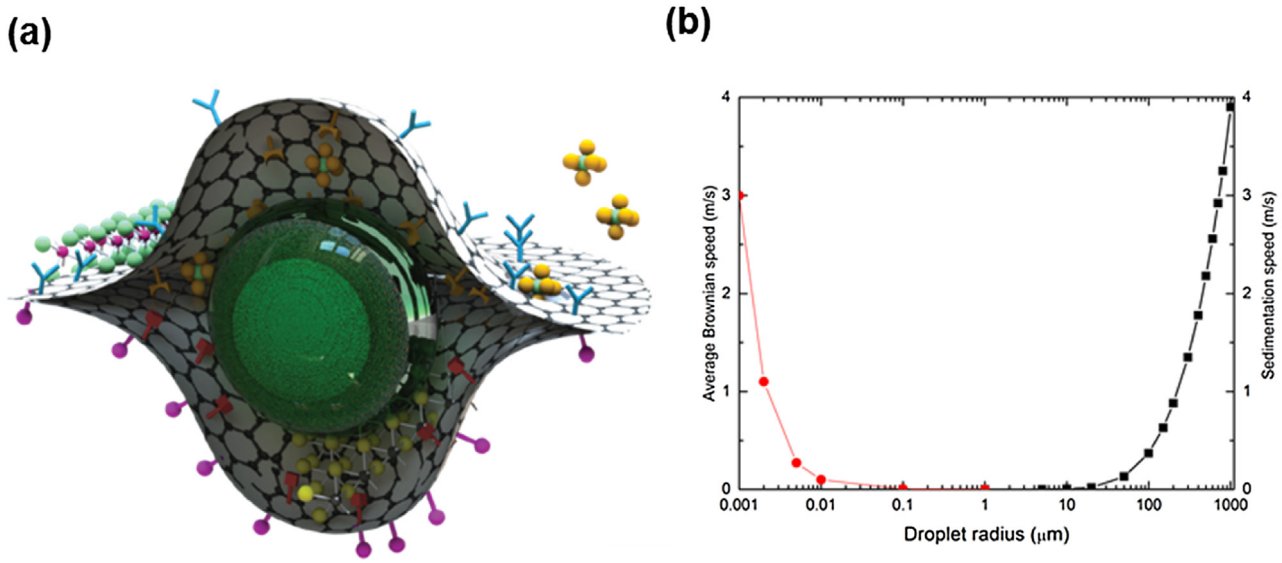

Fig. 15. (a) Syncell concept: 2D material wrapped around a nanoparticle carrier. The particle has four surfaces (two exteriors and two interiors) that can be individually addressed chemically. Additional 2D materials can form complex heterostructures. The outer membrane can have pores, allowing its interior to interact with the particle environment. (b) Sedimentation speed and the average Brownian speed calculations for water droplet at normal conditions, showing that sedimentation speed falls down to almost zero for particles smaller than 50 μm.

rials, these devices are only a few atoms thick, enabling a high integration density.

Due to their high aspect ratio, micrometer-scale 2D materials have a low mechanical stability that limits their application off-substrate. We, therefore, envision novel microparticles and polymer surfaces carrying 2D materials and even 2D circuits (Fig. 15a). Besides integrated electronic properties, these machines can have their 2D layers functionalized with different chemicals, creating a highly asymmetrical particle that is normally difficult to achieve with standard chemical synthesis routes. Size shrinkage down to micrometers will also dramatically decrease sedimentation rates of these particles: compare rates of < 1 cm/s with 1 m/s for millimeter-sized particles falling in the air (Fig. 15b). This can potentially lower (or even completely remove the need) of spending energy on the active movement, enabling the use of micrometer-sized machines in the air and other gaseous environments. Finally, note that the performance of electronic device changes when it is removed from a native substrate due to the imposed stretch and strain [206]; however, 2D materials possess higher strain limits as compared to the conventional III-V materials [207]. Overall, such architectures, as enabled by 2D materials, can yield new benefits to the field of microrobotics, increasing the information and complexity density to those obtained in living cells.

Thermal conduction and applications

The Maxwell model and percolation theory concern isotropic composites; however, fine-tuned manipulation of 2D nanomaterial composites at the nanoscale using macroscopic methods can enable unique thermal properties [208–215]. Consider a stacked graphene/polymer composite (Fig. 16a). For such a composite, shown schematically in the inset, the in-plane and through-plane thermal conductivity can be predicted using resistors in parallel and series models, as shown in Eqs. (5.1) and (5.2), respectively.

$$k_{eff,||} = k_{G,||}\theta_G + k_M(1-\theta_G) \tag{5.1}$$

where $k_{eff,||}$ is the effective thermal conductivity predicted for a resistor in parallel graphene/polymer composite, $k_{G,||}$ is the in-plane thermal conductivity of graphene (3000 W m^{-1} K^{-1}), and θ_G is the volume fraction of graphene [11].

$$k_{eff,\perp} = \frac{k_{G,\perp}k_M}{k_M\theta_G + k_{G,\perp}(1-\theta_G)} \tag{5.2}$$

where $k_{eff,\perp}$ is the effective thermal conductivity predicted for a resistor in series graphene/polymer composite and $k_{G,\perp}$ is the through-plane thermal conductivity of graphene (6 W m^{-1} K^{-1}) [216].

The effective in-plane and through-plane thermal conductivities as a function of graphene volume fraction are shown in Fig. 16a for a graphene/PTFE composite, which can be compared with the graphite/PTFE composite in Fig. 4 of the previous section. The lower end of the range for the in-plane thermal conductivity of graphene and the through-plane thermal conductivity of pyrolytic graphite were chosen for $k_{G,||}$ and $k_{G,\perp}$, respectively. Comparing with Fig. 4 (previous section), the 4^j stacked graphene/PTFE composite - enabled by high area and high-quality 2D materials - is anticipated to yield a very high in-plane thermal conductivity; however, the through-plane effective thermal conductivity of the 4^j composite is quite low. Interestingly, the geometry enabled by the Archimedean scroll fabricated from large area graphene and polycarbonate by Liu et al. has the potential to maintain the high effective thermal conductivity of the 4^j composite while enhancing isotropy.

Fig. 16b shows a schematic of an Archimedean scroll fiber. The XY plane corresponds to the radial direction and the z-axis corresponds to the axial direction. The effective thermal conductivity of a graphene/polymer composite in the axial direction is anticipated to be equal to the in-plane effective thermal conductivity described in Fig. 16a ($k_{eff,||}$). If we consider the heat source (red) located in the center of the Archimedean scroll, it is anticipated that, for a highly anisotropic 2D material with a low thermally conducting matrix, the heat would preferentially spread via travel along the spiral structure. Consequently, we would expect the effective thermal conductivity in the radial direction to exceed the through-plane effective thermal conductivity described in Fig. 16a ($k_{eff,\perp}$). Overall, in comparison with the 4^j composite described in Fig. 16a – characterized by $k_{eff,||}$ in two directions and $k_{eff,\perp}$ in the third direction – the Archimedean scroll is characterized by $k_{eff,||}$ in one

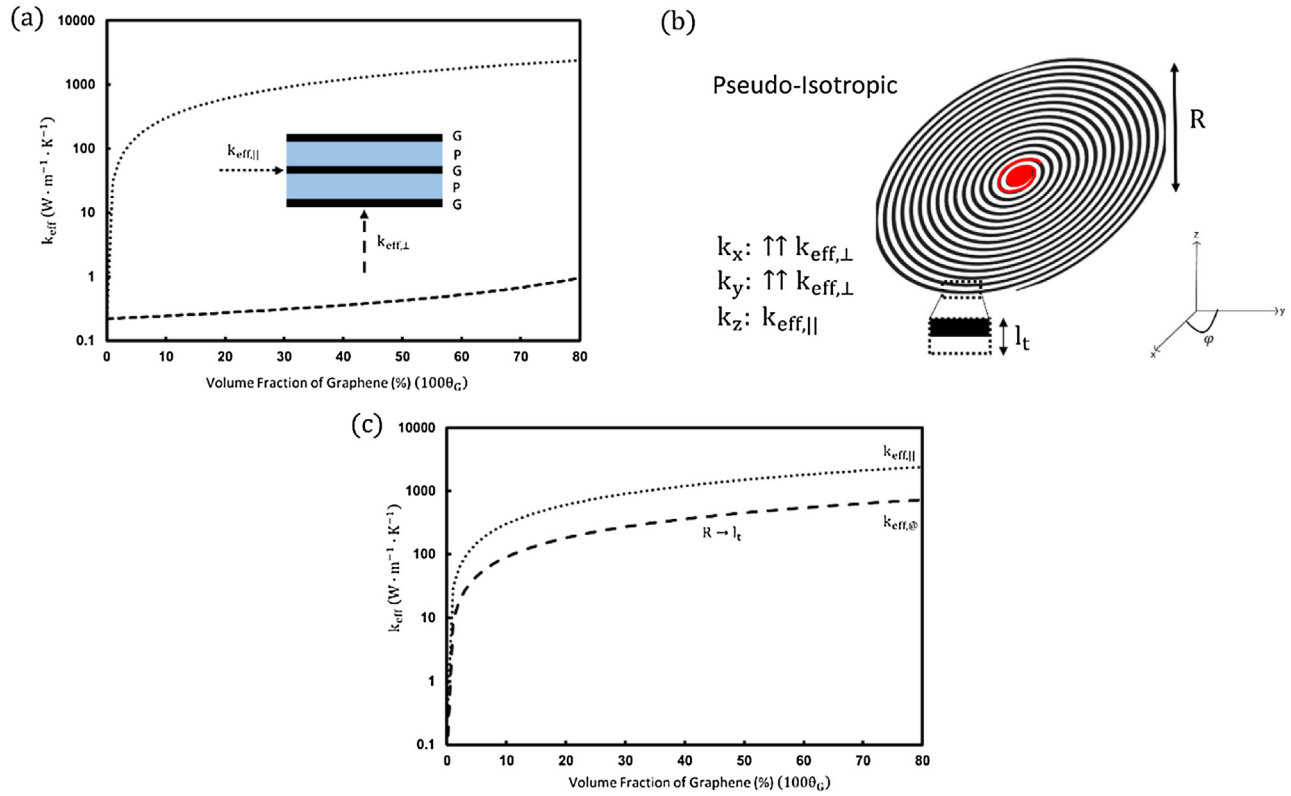

Fig. 16. (a) Effective thermal conductivity for the in-plane $\left(k_{eff,||}\right)$ and through-plane ($k_{eff,\perp}$) directions of a graphene (G) and PTFE (P) composite as a function of the graphene content. Thermal conductivity of the PTFE matrix [55]: $k_M = 0.22\,W\,m^{-1}\,K^{-1}$. Reprinted with permission from SAGE Journals. Copyright (2010) SAGE Journals. In-plane thermal conductivity of graphene [11]: $k_{G,||} = 3000\,W\,m^{-1}\,K^{-1}$. Through-plane thermal conductivity of graphene [216]: $k_{G,\perp} = 6\,W\,m^{-1}\,K^{-1}$. (b) A cartoon depicting graphene arranged into an Archimedean scroll structure and exposed to a point heat source at its center. High effective thermal conductivity $\left(k_{eff,||}\right)$ is preserved in the axial (z) direction, while the scrolling of the 2D material enhances thermal conduction in the XY plane beyond $k_{eff,\perp}$. (c) Calculations predicting the enhancement in thermal conductivity in the XY plane ($k_{eff,@}$) for a graphene Archimedean scroll with $R \sim l_t$, illustrating a pseudo-isotropic behavior.

direction and a radial effective thermal conductivity in excess of $k_{eff,\perp}$. While one dimension of high effective thermal conductivity is lost in transitioning from a 4^j composite to the Archimedean scroll, the scroll is anticipated to be pseudo-isotropic with excellent axial thermal conductivity and respectable radial thermal conductivity. Using a simple steady-state effective resistor model, we can predict the enhancement of the radial thermal conductivity due to the scrolling of a graphene/polymer composite. Equation (5.3) gives the radius for an Archimedean scroll as a function of the angle through which the composite has been scrolled.

$$r = b\varphi \tag{5.3}$$

where b is the change in radius (l_t) per full rotation, as shown in Eq. (5.4).

$$b = \frac{l_t}{2\pi} \tag{5.4}$$

The total length (L) of the graphene scrolled to construct an Archimedean scroll of final radius R is then given by Eq. (5.5).

$$L = \frac{l_t}{2\pi}\int_0^{\frac{2\pi R}{l_t}} \sqrt{\varphi^2 + 1}\, d\varphi \tag{5.5}$$

To predict the limit of this fabrication methodology for enhancing the radial thermal conductivity, we can make the assumption that the final radius of the scroll is on the order of the layer thickness of the scroll:

$$R \sim l_t \tag{5.6}$$

Assuming that the graphene is highly thermally conductive relative to the polymer matrix, such that heat flow occurs is a spiral fashion without leakage between layers, Eq. (5.7) describes the effective thermal conductivity in the radial direction ($k_{eff,@}$).

$$\frac{R}{k_{eff,@}} = \frac{L}{k_{eff,||}} \tag{5.7}$$

Simplifying Eq. (5.7) with Eqs. (5.5) and (5.6), we obtain a simple expression for the effective thermal conductivity in the radial direction as a function of the effective in-plane thermal conductivity of the comparable 4^j composite:

$$k_{eff,@} \approx 0.3\, k_{eff,||} \tag{5.8}$$

Using Eq. (5.8) and the values for the in-plane effective thermal conductivity of the 4^j composite from Fig. 16a, we show the predicted effective thermal conductivity in the radial direction for a graphene/PTFE Archimedean scroll (Fig. 16c), which is a substantial improvement in comparison with the through-plane effective thermal conductivity of the 4^j composite. It should be noted that the simple model proposed above neglects phonon scattering, which could prove problematic at high volume fractions of graphene – at which point the layer thickness and radius of the scroll would be quite small and likely approach the bulk phonon mean free path of graphene (~ 700 nm), resulting in phonon scattering at the curvature [56]. The model also neglects leakage between the layers, which would likely enhance the effective radial thermal conductivity.

Overall, large area 2D nanomaterial-based composites have unique opportunities in the field of thermal transport. In isotropic

Please cite this article in press as: P. Liu, et al., Emerging trends in 2D nanotechnology that are redefining our understanding of "Nanocomposites", Nano Today (2018), https://doi.org/10.1016/j.nantod.2018.04.012

composites that are well represented by the Maxwell model and percolation theory, large area 2D nanomaterials will absolutely result in enhanced thermal transport. However, it is likely that the most interesting impact of large area 2D nanomaterials will be for highly ordered composite materials, due to the ease of ordering large area 2D materials at the nanoscale using macroscopic methods. Nanomaterial-based composites such as the Archimedean scroll and 4^j stack developed by Liu et al. from large area graphene and spin-coated polymer thin films are two examples of such composites, which could give rise to very interesting thermal properties.

Optical properties and applications

In addition to their good transparency, layered composites with 2D materials and polymers also have optical applications. A periodic structure of two materials different refractive indices along one axis with a period comparable to the wavelength of light forms a 1D photonic crystal [217]. Such a periodic structure forbids certain wavelengths of light to propagate in the material. There are reports on 1D photonic crystals based on graphene/PMMA [218,219], MoS_2/PMMA and WS_2/PMMA [220] for the potential application of sensors [219], fluorescence emission enhancement, and modulators [218]. Yan et al. patterned a graphene/polymer layer by layer stack into microdisk arrays and demonstrated tunable far-infrared notch filters and terahertz linear polarizers [221]. These works provide feasibility to realize more complex 1D to 3D photonic structures for various optical application in wide ranges of wavelength from visible to terahertz.

A single quantum emitter in 2D materials: an emerging field in 2D materials is single photon emitter (SPE), which is a central part of quantum information technologies. Up to the present time, that of solid state is restricted in 0D [222], 1D [223,224], and 3D [225], while 2D has been missing. However, in defects of monolayer WSe_2 [226–228], single photon emission has been reported. The advantage of a 2D quantum emitter is its easy integration into a photonic circuit and the efficient photon extraction. Although diamond NV center is one of the most extensively studied, the challenge has been the integration of SPE with optical cavities, as photonic integration with the couple to plasmonic resonators or photonic cavity requires proximity in nano-scale. A typical solid state emitter embedded in a bulk host, such as a diamond NV center, suffers from internal reflection, resulting in photon loss. On the other hand, 2D materials allow to couple with optical cavity [229–233] and directly extract photon.

The most recent discovery in the class of 2D single photon emitters is the NV center of hexagonal boron nitride (hBN) (Fig. 17a–c) [234]. The SPEs in hBN exhibit the highest count rate of photon emission among solid state SPEs (3×10^6 counts/s) [235]. Another benefit of hBN SPEs is stable room-temperature operation attributed to deep states. Optically active defects are introduced in the host crystal of hBN using e-beam irradiation [236], ion-implantation of B, BN, O, Si [236], He, N ion [237], annealing [234], laser ablation [236], chemical etching with peroxymonosulfuric acid (H_2O_2:H_2SO_4) accompanied by H_2SO_4:H_3PO_4 [237], and Ar plasma etching [238]. The photoemission of zero phonon line spans the range of nIR to visible (Fig. 17d)) [239]. The 2D structure facilitates to modulate emission properties, applying external strain [240].

The stability of SPEs in hBN at room temperature expands the potential application to sensing and imaging under ambient conditions as well as quantum information technology. As a similar structure to hBN - in that the optically active vacancy is in the insulator host - nanodiamond NV centers have been employed to detect biological processes because of their non-toxic nature and capability of single molecule detection [241–244]. Although a study of the biocompatibility and nanotoxicity for hBN is still in its primary stage [245], its chemically stable nature is promising for the biological application. A reasonable approach to introduce nanodiamond into a cell is surface engineering of the NV center with polymer composite [246–248]. Rendler et al. proposed a composite of polymer and nanodiamond that allows the detection of changes in pH and redox potential in the local environment by monitoring spin relaxation [248]. Manipulating hBN surface chemistry could expand the functions for selective sensing in chemical and biological environments.

Conclusion and outlook

In this review paper, we have highlighted the use of large-area 2D materials, graphene mainly, as nanoinclusions for composite materials to achieve a maximum reinforcement in terms of mechanical properties, barrier performance, electrical/thermal conduction, and optical properties. This was discussed from both theoretical and experimental aspects. Large-area 2D sheets can be produced via top-down exfoliation and bottom-up CVD method. The further dispersion of these large-area 2D materials into matrix materials, mainly polymers, has been also presented. Instead of a traditional vigorous solution or melt mixing, elegant methods such as *in-situ* polymerization, layer-by-layer assembly and their continuous processes like vacuum-assisted filtration or evaporation can be used for the exfoliated 2D materials without crumple or crack the large-area sheets. For 2D material grown by CVD methods,

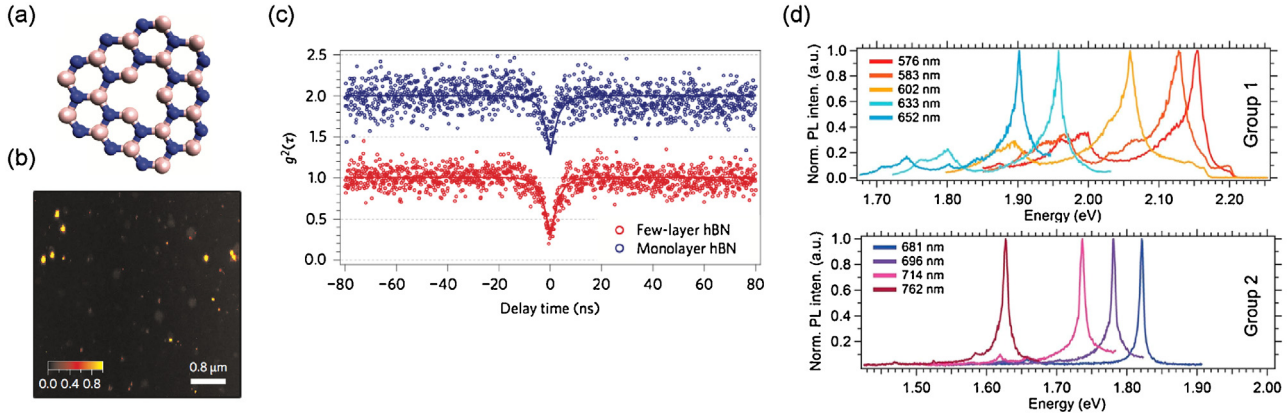

Fig. 17. Optical properties of single photon emitter in hBN. (a) Schematic image of hBN vacancy. (b) PL spatial mapping of hBN particles. (c) Second-order autocorrelation functions of few- and mono-layer hBN. (d) Multicolor PL spectra. Figures (a, b, c) are reproduced (adapted) with the permission from [234]. Copyright (2016) Springer Nature. Figure (d) is reproduced (adapted) with permission from [239]. Copyright (2016) American Chemical Society.

Please cite this article in press as: P. Liu, et al., Emerging trends in 2D nanotechnology that are redefining our understanding of "Nanocomposites", Nano Today (2018), https://doi.org/10.1016/j.nantod.2018.04.012

after transferring them to polymer films, a further folding, cutting, stacking, and/or scrolling can render exotic nanocomposites with the continuous 2D sheet that spans completely across the physical dimension of the composite body.

Later, we have been mainly focused on the nanocomposite system with continuous 2D materials grown CVD. The recently developed 4^j stacking and transverse shear scrolling scales up the fabrication, making the whole process modular, so that the composition of the final nanocomposite remains the same as the starting thin polymer film layers during the scaling up. This enables a controlled alignment and positioning of the 2D layer in the nanocomposite body, generating layered and scrolled nanocomposites with theoretically predicted mechanical and electrical enhancements. These composite samples with well-defined microstructures, on the one hand, can be used as standard samples to study the fundamental mechanism of the reinforcement in the aspects of mechanics, barrier properties, electrical conduction, thermal transport, and optical properties (like nanophotonics). On the other hand, these nanocomposites with a given spatial distribution of the 2D sheets within the matrix have the potential to be used in various functional components, such as capacitor, inductor, particle state machines, and 2D single photon emitter. With these, we emphasize and outlook a few important emerging aspects that, we hope, will intrigue the 2D nanocomposite community in the future, enabling a bright future of the nanocomposites with large-area 2D materials:

(1) For polymer nanocomposites with a small amount of nanonclusions, the changes of their mechanical properties stem from two contributions: one is the modification of matrix and the other is the direct mechanical reinforcement by the nanofillers. The matrix modification effect can be found in many other types of nanofillers, such as nanoclays, silica nanoparticles, metal oxide nanoparticles. Only the second contribution from the nanoparticles themselves can distinguish one nanofiller from others and identify the differences between nanoparticles. 2D materials, like graphene, have their advantage when considering that carbon-carbon sp^2 hybridized bond is the nature's strongest. To achieve a maximum reinforcement from the 2D nanofillers, a good interfacial binding to facilitate the stress transfer is necessary. Further interface engineering via chemical modification or other methods to enhance such a binding will be the next important direction, and this has been also highlighted by Zhang and Samorì recently [154]. Under such conditions, the study of the stress transfer, mechanical deformation, elongation, and failure behavior of these standard and modular composites will be quite meaningful, providing a deeper understanding of the reinforcement mechanism.
(2) For composites with the exfoliated 2D materials as major components, i.e. those nacre-liked structural materials, in addition to promoting the interfacial binding via a synergistic engineering of the interface chemistry, as highlighted by a recent paper from Zhang et al. [144], a study of using large-area 2D layer with higher aspect ratio, at the same time, should witness a further mechanical reinforcement. When overlooking the whole process with graphene as an example, we start from graphite, and exfoliate it to 2D graphene or graphene oxide nanoflakes, after certain chemical treatment, we assemble them back to 3D composite body again. In this process, the really important element we add is a strong binding between graphene layers, when comparing the weak inter-layer van der Waals (vdW) bonding, low shear strength of the raw graphite and their application as solid lubricants [249]. On the other side, we need to maintain the pristine geometry (i.e. size) and properties (i.e. less defects) of the graphene units as much as possible, although this is always in contradiction of the harsh environments 2D materials experience with high shear force and strong chemical reactions.
(3) The scrolled fiber also represents a completely new concept of nanocomposite fabrication, dimension transformation from 2D to 3D, a three-dimensional (3D) composite body comprised exclusively of 2D topology. With such a construction concept, many of the exotic electrical, photonic and photoelectric properties of 2D materials and their heterojunctions can transfer from 2D plane to 3D objects via a simple fabrication, scrolling, or folding more generally, and other methods. At the same time, the 3D topology may also bring new functions that may not exist at 2D: for example, inductor of the scroll structure and state particle machine.
(4) The last and arguably the most important is the scalability of the process and final products. Actually, the scalability is always a critical bottleneck in the research of nanomaterials that one must overcome to make a tangible impact in the real world. The 2D to 3D transformation, such as folding or scrolling, has the advantage that the macroscopic 3D object can have the same structural control as their 2D source at atomic and molecular levels, in sharp contrast to the loss of control of many other processes [25]. Now, a major challenge is how to produce and transfer lager-area, high-quality 2D materials at scale and lower cost. Fortunately, the production cost of 2D materials with CVD technique is continuously reducing and their transfer process has been also improved a lot, roll-to-roll production and transfer for example, with an annual production capacity of 110 K m^2 at 2014 and about million m^2 at 2016 only in China [250]. Scalable synthesis of 2D materials via wet chemistry method also is developing fast, promising a diversity of new 2D materials for nanocomposite application. In particular, a significant progress has been achieved in the bottom-up synthesis of 2D polymers and covalent organic framework in the last decade, various thin 2D polymer layers have been reported [251,252]. A number of methods, like interfacial or surface polymerization, either solid/liquid surface [253,254], liquid/liquid interface, or gas/liquid surface [255–257], single-crystal-to-single-crystal (scsc) method (crystal engineering) [258–261], the exfoliation of COF [262], and solid-state topochemical polymerizations have been reported. These thin layers of 2D polymers, by tuning their chemical composition, can be designed to have outstanding mechanical properties, catalysis capability, semiconducting performance, and so on. Obviously, this will be an important direction, since it gives more freedom to tune the structure and performance for researcher to design their 2D thin sheets as building blocks for the further nanocomposite construction with the versatile combination of functions and complexities.

In addition to the scale of 2D materials production, another angle to consider the scalability is to reduce the required amount of 2D materials in the nanocomposite materials [155]. Usage of large-area, high-quality 2D material can significantly lower this amount [263,264]. For example, the materials will be conductive if the surface layer covered with graphene or only a few layers of graphene embedded in the matrix [43], and only a single layer or few layers of graphene on the surface of the polymer film is required to achieve good barrier performance against water vapor.

Acknowledgments

This work was primarily funded by 2015 US Office of Naval Research Multi University Research Initiative (MURI) grant on Foldable and Adaptive Two-Dimensional Electronics (FATE) at MIT, Harvard and South California University. P. L. thanks the funding from "One-hundred Talents Program" of Zhejiang University. D. K.

Please cite this article in press as: P. Liu, et al., Emerging trends in 2D nanotechnology that are redefining our understanding of "Nanocomposites", Nano Today (2018), https://doi.org/10.1016/j.nantod.2018.04.012

is supported by the Grant-in-Aid for JSPS Fellows (JSPS KAKENHI Grant Number 15J07423) and Encouragement of Young Scientists (B) (JSPS KAKENHI Grant Number JP16K17485) from Japan Society for the Promotion of Science. V.B.K.is supported by The Swiss National Science Foundation (project no.P300P2_174469).

References

[1] K.S. Novoselov, A.K. Geim, S.V. Morozov, D. Jiang, Y. Zhang, S.V. Dubonos, et al., Science 306 (2004) 666–669.
[2] K.S. Novoselov, D. Jiang, F. Schedin, T.J. Booth, V.V. Khotkevich, S.V. Morozov, et al., Proc. Natl. Acad. Sci. U. S. A. 102 (2005) 10451–10453.
[3] S.Z. Butler, S.M. Hollen, L. Cao, Y. Cui, J.A. Gupta, H.R. Gutiérrez, et al., ACS Nano 7 (2013) 2898–2926.
[4] A.C. Ferrari, F. Bonaccorso, V. Fal'ko, K.S. Novoselov, S. Roche, P. Boggild, et al., Nanoscale 7 (2015) 4598–4810.
[5] H. Zhang, ACS Nano 9 (2015) 9451–9469.
[6] C. Tan, X. Cao, X.-J. Wu, Q. He, J. Yang, X. Zhang, et al., Chem. Rev. 117 (2017) 6225–6331.
[7] C. Lee, X. Wei, J.W. Kysar, J. Hone, Science 321 (2008) 385–388.
[8] G.-H. Lee, R.C. Cooper, S.J. An, S. Lee, A. van der Zande, N. Petrone, et al., Science 340 (2013) 1073–1076.
[9] K.I. Bolotin, K.J. Sikes, Z. Jiang, M. Klima, G. Fudenberg, J. Hone, et al., Solid State Commun. 146 (2008) 351–355.
[10] A.A. Balandin, S. Ghosh, W. Bao, I. Calizo, D. Teweldebrhan, F. Miao, et al., Nano Lett. 8 (2008) 902–907.
[11] S. Ghosh, I. Calizo, D. Teweldebrhan, E.P. Pokatilov, D.L. Nika, A.A. Balandin, et al., Appl. Phys. Lett. 92 (2008) 151911.
[12] W. Cai, A.L. Moore, Y. Zhu, X. Li, S. Chen, L. Shi, et al., Nano Lett. 10 (2010) 1645–1651.
[13] X. Xu, L.F.C. Pereira, Y. Wang, J. Wu, K. Zhang, X. Zhao, et al., Nat. Commun. 5 (2014) 3689.
[14] J.-U. Lee, D. Yoon, H. Kim, S.W. Lee, H. Cheong, Phys. Rev. B 83 (2011) 081419.
[15] A.A. Balandin, Nat. Mater. 10 (2011) 569.
[16] D.L. Nika, A.A. Balandin, Rep. Prog. Phys. 80 (2017) 036502.
[17] Y. Liu, N.O. Weiss, X. Duan, H.-C. Cheng, Y. Huang, X. Duan, Nat. Rev. Mater. 1 (2016) 16042.
[18] Q.H. Wang, K. Kalantar-Zadeh, A. Kis, J.N. Coleman, M.S. Strano, Nat. Nanotechnol. 7 (2012) 699–712.
[19] G. Fiori, F. Bonaccorso, G. Iannaccone, T. Palacios, D. Neumaier, A. Seabaugh, et al., Nat. Nanotechnol. 9 (2014) 768–779.
[20] X. Zhang, L. Hou, A. Ciesielski, P. Samorì, Adv. Energy Mater. 6 (2016), 1600671-n/a.
[21] K.S. Novoselov, A. Mishchenko, A. Carvalho, A.H. Castro Neto, Science (2016) 353.
[22] M.-Y. Li, C.-H. Chen, Y. Shi, L.-J. Li, Mater. Today 19 (2016) 322–335.
[23] A. Gupta, T. Sakthivel, S. Seal, Prog. Mater. Sci. 73 (2015) 44–126.
[24] R. Mas-Balleste, C. Gomez-Navarro, J. Gomez-Herrero, F. Zamora, Nanoscale 3 (2011) 20–30.
[25] Nat. Nanotechnol. 11 (2016) 733.
[26] H. Kim, A.A. Abdala, C.W. Macosko, Macromolecules 43 (2010) 6515–6530.
[27] T. Kuilla, S. Bhadra, D. Yao, N.H. Kim, S. Bose, J.H. Lee, Prog. Polym. Sci. 35 (2010) 1350–1375.
[28] J.R. Potts, D.R. Dreyer, C.W. Bielawski, R.S. Ruoff, Polymer 52 (2011) 5–25.
[29] R. Verdejo, M.M. Bernal, L.J. Romasanta, M.A. Lopez-Manchado, J. Mater. Chem. 21 (2011) 3301–3310.
[30] X. Huang, X. Qi, F. Boey, H. Zhang, Chem. Soc. Rev. 41 (2012) 666–686.
[31] R.J. Young, I.A. Kinloch, L. Gong, K.S. Novoselov, Compos. Sci. Technol. 72 (2012) 1459–1476.
[32] T.K. Das, S. Prusty, Polym. Plast. Technol. Eng. 52 (2013) 319–331.
[33] K. Hu, D.D. Kulkarni, I. Choi, V.V. Tsukruk, Prog. Polym. Sci. 39 (2014) 1934–1972.
[34] M. Zhang, Y. Li, Z. Su, G. Wei, Polym. Chem. 6 (2015) 6107–6124.
[35] L. Gong, I.A. Kinloch, R.J. Young, I. Riaz, R. Jalil, K.S. Novoselov, Adv. Mater. 22 (2010) 2694–2697.
[36] C.L. Tucker Iii, E. Liang, Compos. Sci. Technol. 59 (1999) 655–671.
[37] H. Liu, L.C. Brinson, Compos. Sci. Technol. 68 (2008) 1502–1512.
[38] P. May, U. Khan, A. O'Neill, J.N. Coleman, J. Mater. Chem. 22 (2012) 1278–1282.
[39] T. Mori, K. Tanaka, Acta Metall. 21 (1973) 571–574.
[40] G.P. Tandon, G.J. Weng, Polym. Compos. 5 (1984) 327–333.
[41] J.C.H. Affdl, J.L. Kardos, Polym. Eng. Sci. 16 (1976) 344–352.
[42] J. Li, J.-K. Kim, Compos. Sci. Technol. 67 (2007) 2114–2120.
[43] P. Liu, Z. Jin, G. Katsukis, L.W. Drahushuk, S. Shimizu, C.-J. Shih, et al., Science 353 (2016) 364–367.
[44] T.D. Fornes, D.R. Paul, Polymer 44 (2003) 4993–5013.
[45] M. Van Es, F. Xiqiao, J. Van Turnhout, E. Van der Giessen, Comparing Polymer-Clay Nanocomposites With Conventional Composites Using Composite Modeling, Speciality Polymer Additives: Principles and Applications, Blackwell Science, CA Malden, MA, 2001, Chapter 21.
[46] J.S. Bunch, S.S. Verbridge, J.S. Alden, A.M. van der Zande, J.M. Parpia, H.G. Craighead, et al., Nano Lett. 8 (2008) 2458–2462.
[47] S. Hu, M. Lozada-Hidalgo, F.C. Wang, A. Mishchenko, F. Schedin, R.R. Nair, et al., Nature 516 (2014) 227–230.
[48] E.L. Cussler, S.E. Hughes, W.J. Ward III, R. Aris, J. Membr. Sci. 38 (1988) 161–174.
[49] C. Lu, Y.-W. Mai, Phys. Rev. Lett. 95 (2005) 088303.
[50] L.E. Nielsen, J. Macromol. Sci., Pure Appl. Chem. 1 (1967) 929–942.
[51] Y. Cui, S. Kundalwal, S. Kumar, Carbon 98 (2016) 313–333.
[52] J. Hicks, A. Behnam, A. Ural, Appl. Phys. Lett. 95 (2009) 213103.
[53] D. Stauffer, A. Aharony, Introduction to Percolation Theory, Taylor and Francis, London and Philadelphia, 1994.
[54] A. Celzard, E. McRae, C. Deleuze, M. Dufort, G. Furdin, J.F. Marêché, Phys. Rev. B 53 (1996) 6209–6214.
[55] G. Zhang, Y. Xia, H. Wang, Y. Tao, G. Tao, S. Tu, et al., J. Compos. Mater. 44 (2010) 963–970.
[56] K.M.F. Shahil, A.A. Balandin, Nano Lett. 12 (2012) 861–867.
[57] G.R. Bhimanapati, Z. Lin, V. Meunier, Y. Jung, J. Cha, S. Das, et al., ACS Nano 9 (2015) 11509–11539.
[58] J. Yu, J. Li, W. Zhang, H. Chang, Chem. Sci. 6 (2015) 6705–6716.
[59] W. Fang, A.L. Hsu, Y. Song, J. Kong, Nanoscale 7 (2015) 20335–20351.
[60] J. Li, M. Östling, Electronics 4 (2015) 1033.
[61] L. Zhong, M. Amber, B. Natalie, S. Shruti, Z. Kehao, S. Yifan, et al., 2D Mater. 3 (2016) 042001.
[62] X.-H. Lin, J.-G. Gai, RSC Adv. 6 (2016) 17818–17844.
[63] Q. He, H.G. Sudibya, Z. Yin, S. Wu, H. Li, F. Boey, et al., ACS Nano 4 (2010) 3201–3208.
[64] Q. He, S. Wu, S. Gao, X. Cao, Z. Yin, H. Li, et al., ACS Nano 5 (2011) 5038–5044.
[65] Y. Hernandez, V. Nicolosi, M. Lotya, F.M. Blighe, Z. Sun, S. De, et al., Nat. Nanotechnol. 3 (2008) 563–568.
[66] K.R. Paton, E. Varrla, C. Backes, R.J. Smith, U. Khan, A. O'Neill, et al., Nat. Mater. 13 (2014) 624–630.
[67] Y. Lv, L. Yu, C. Jiang, S. Chen, Z. Nie, RSC Adv. 4 (2014) 13350–13354.
[68] A.M. Abdelkader, A.J. Cooper, R.A.W. Dryfe, I.A. Kinloch, Nanoscale 7 (2015) 6944–6956.
[69] W. Fu, J. Kiggans, S.H. Overbury, V. Schwartz, C. Liang, Chem. Commun. 47 (2011) 5265–5267.
[70] A.B. Bourlinos, V. Georgakilas, R. Zboril, T.A. Steriotis, A.K. Stubos, Small 5 (2009) 1841–1845.
[71] T. Szabó, O. Berkesi, P. Forgó, K. Josepovits, Y. Sanakis, D. Petridis, et al., Chem. Mater. 18 (2006) 2740–2749.
[72] M. Lotya, P.J. King, U. Khan, S. De, J.N. Coleman, Acs Nano 4 (2010) 3155–3162.
[73] A.J. Mannix, B. Kiraly, M.C. Hersam, N.P. Guisinger, Nat. Rev. Chem. 1 (2017) 0014.
[74] G.M. Morales, P. Schifani, G. Ellis, C. Ballesteros, G. Martinez, C. Barbero, et al., Carbon 49 (2011) 2809–2816.
[75] Y. Hernandez, M. Lotya, D. Rickard, S.D. Bergin, J.N. Coleman, Langmuir (2010) 26.
[76] S. De, P.J. King, M. Lotya, A. O'Neill, E.M. Doherty, Y. Hernandez, et al., Small 6 (2010) 458–464.
[77] A.S. Wajid, S. Das, F. Irin, H.S.T. Ahmed, J.L. Shelburne, D. Parviz, et al., Carbon 50 (2012) 526–534.
[78] Q. Su, S. Pang, V. Alijani, C. Li, X. Feng, K. Muellen, Adv. Mater. 21 (2009), 3191-+.
[79] D. Parviz, S. Das, H.S.T. Ahmed, F. Irin, S. Bhattacharia, M.J. Green, Acs Nano 6 (2012) 8857–8867.
[80] W.S. Hummers, R.E. Offeman, J. Am. Chem. Soc. 80 (1958) 1339.
[81] D.R. Dreyer, S. Park, C.W. Bielawski, R.S. Ruoff, Chem. Soc. Rev. 39 (2010).
[82] S. Stankovich, R.D. Piner, X. Chen, N. Wu, S.T. Nguyen, R.S. Ruoff, J. Mater. Chem. 16 (2006) 155–158.
[83] S. Stankovich, D.A. Dikin, R.D. Piner, K.A. Kohlhaas, A. Kleinhammes, Y. Jia, et al., Carbon 45 (2007) 1558–1565.
[84] C.T.J. Low, F.C. Walsh, M.H. Chakrabarti, M.A. Hashim, M.A. Hussain, Carbon 54 (2013) 1–21.
[85] K. Parvez, Z.-S. Wu, R. Li, X. Liu, R. Graf, X. Feng, et al., J. Am. Chem. Soc. 136 (2014) 6083–6091.
[86] K. Parvez, R.J. Li, S.R. Puniredd, Y. Hernandez, F. Hinkel, S.H. Wang, et al., Acs Nano 7 (2013) 3598–3606.
[87] N. Liu, P. Kim, J.H. Kim, J.H. Ye, S. Kim, C.J. Lee, ACS Nano 8 (2014) 6902–6910.
[88] A.A. Green, M.C. Hersam, Nano Lett. 9 (2009) 4031–4036.
[89] C. Backes, B.M. Szydlowska, A. Harvey, S.J. Yuan, V. Vega-Mayoral, B.R. Davies, et al., ACS Nano 10 (2016) 1589–1601.
[90] J. Kang, V.K. Sangwan, J.D. Wood, M.C. Hersam, Acc. Chem. Res. 50 (2017) 943–951.
[91] X. Li, W. Cai, J. An, S. Kim, J. Nah, D. Yang, et al., Science 324 (2009) 1312–1314.
[92] K.S. Kim, Y. Zhao, H. Jang, S.Y. Lee, J.M. Kim, K.S. Kim, et al., Nature 457 (2009) 706–710.
[93] A. Reina, X. Jia, J. Ho, D. Nezich, H. Son, V. Bulovic, et al., Nano Lett. 9 (2009) 30–35.
[94] Z. Tu, Z. Liu, Y. Li, F. Yang, L. Zhang, Z. Zhao, et al., Carbon 73 (2014) 252–258.
[95] Y. Hao, M.S. Bharathi, L. Wang, Y. Liu, H. Chen, S. Nie, et al., Science 342 (2013) 720–723.
[96] A. Cabrero-Vilatela, R.S. Weatherup, P. Braeuninger-Weimer, S. Caneva, S. Hofmann, Nanoscale 8 (2016) 2149–2158.
[97] C. Mattevi, H. Kim, M. Chhowalla, J. Mater. Chem. 21 (2011) 3324–3334.
[98] R. Muñoz, C. Gómez-Aleixandre, Chem. Vap. Deposition 19 (2013) 297–322.

Please cite this article in press as: P. Liu, et al., Emerging trends in 2D nanotechnology that are redefining our understanding of "Nanocomposites", Nano Today (2018), https://doi.org/10.1016/j.nantod.2018.04.012

[99] Y.-H. Lee, X.-Q. Zhang, W. Zhang, M.-T. Chang, C.-T. Lin, K.-D. Chang, et al., Adv. Mater. 24 (2012) 2320–2325.
[100] Y. Shi, H. Li, L.-J. Li, Chem. Soc. Rev. 44 (2015) 2744–2756.
[101] Q. Ji, Y. Zhang, Y. Zhang, Z. Liu, Chem. Soc. Rev. 44 (2015) 2587–2602.
[102] M. Bosi, RSC Adv. 5 (2015) 75500–75518.
[103] L. Song, L. Ci, H. Lu, P.B. Sorokin, C. Jin, J. Ni, et al., Nano Lett. 10 (2010) 3209–3215.
[104] Y. Shi, C. Hamsen, X. Jia, K.K. Kim, A. Reina, M. Hofmann, et al., Nano Lett. 10 (2010) 4134–4139.
[105] A. Ismach, H. Chou, D.A. Ferrer, Y. Wu, S. McDonnell, H.C. Floresca, et al., ACS Nano 6 (2012) 6378–6385.
[106] K.K. Kim, A. Hsu, X. Jia, S.M. Kim, Y. Shi, M. Hofmann, et al., Nano Lett. 12 (2012) 161–166.
[107] Z. Liu, L. Song, S. Zhao, J. Huang, L. Ma, J. Zhang, et al., Nano Lett. 11 (2011) 2032–2037.
[108] Y. Chen, X.L. Gong, J.G. Gai, Adv. Sci. 3 (2016).
[109] H. An, W.J. Lee, J. Jung, Curr. Appl. Phys. 11 (2011) S81–S85.
[110] L. Gao, W. Ren, H. Xu, L. Jin, Z. Wang, T. Ma, et al., Nat. Commun. (2012) 3.
[111] X. Li, Y. Zhu, W. Cai, M. Borysiak, B. Han, D. Chen, et al., Nano Lett. 9 (2009) 4359–4363.
[112] X. Liang, B.A. Sperling, I. Calizo, G. Cheng, C.A. Hacker, Q. Zhang, et al., ACS Nano 5 (2011) 9144–9153.
[113] J. Kang, S. Hwang, J.H. Kim, M.H. Kim, J. Ryu, S.J. Seo, et al., ACS Nano 6 (2012) 5360–5365.
[114] K.S. Kim, Y. Zhao, H. Jang, S.Y. Lee, J.M. Kim, K.S. Kim, et al., Nature 457 (2009) 706–710.
[115] S. Bae, H. Kim, Y. Lee, X. Xu, J.S. Park, Y. Zheng, et al., Nat. Nanotechnol. 5 (2010) 574–578.
[116] J.W. Suk, A. Kitt, C.W. Magnuson, Y. Hao, S. Ahmed, J. An, et al., ACS Nano 5 (2011) 6916–6924.
[117] L.G.P. Martins, Y. Song, T. Zeng, M.S. Dresselhaus, J. Kong, P.T. Araujo, Proc. Natl. Acad. Sci. U. S. A. 110 (2013) 17762–17767.
[118] H. Park, P.R. Brown, V. Bulović, J. Kong, Nano Lett. 12 (2012) 133–140.
[119] J. Song, F.Y. Kam, R.Q. Png, W.L. Seah, J.M. Zhuo, G.K. Lim, et al., Nat. Nanotechnol. 8 (2013) 356–362.
[120] Z. Lin, Y. Zhao, C. Zhou, R. Zhong, X. Wang, Y.H. Tsang, et al., Sci. Rep. (2015) 5.
[121] D. Ma, J. Shi, Q. Ji, K. Chen, J. Yin, Y. Lin, et al., Nano Res. 8 (2015) 3662–3672.
[122] H. Li, J. Wu, X. Huang, Z. Yin, J. Liu, H. Zhang, ACS Nano 8 (2014) 6563–6570.
[123] A. Gurarslan, Y. Yu, L. Su, Y. Yu, F. Suarez, S. Yao, et al., ACS Nano 8 (2014) 11522–11528.
[124] W. Jung, D. Kim, M. Lee, S. Kim, J.H. Kim, C.S. Han, Adv. Mater. 26 (2014) 6394–6400.
[125] Z.Y. Juang, C.Y. Wu, A.Y. Lu, C.Y. Su, K.C. Leou, F.R. Chen, et al., Carbon 48 (2010) 3169–3174.
[126] E.H. Lock, M. Baraket, M. Laskoski, S.P. Mulvaney, W.K. Lee, P.E. Sheehan, et al., Nano Lett. 12 (2012) 102–107.
[127] B. Marta, C. Leordean, T. Istvan, I. Botiz, S. Astilean, Appl. Surf. Sci. 363 (2016) 613–618.
[128] G.J.M. Fechine, I. Martin-Fernandez, G. Yiapanis, R. Bentini, E.S. Kulkarni, R.V. Bof De Oliveira, et al., Carbon 83 (2015) 224–231.
[129] B.J. Carey, J.Z. Ou, R.M. Clark, K.J. Berean, A. Zavabeti, A.S.R. Chesman, et al., Nat. Commun. 8 (2017) 14482.
[130] Y.D. Kim, J. Hone, Nature 544 (2017) 167–168.
[131] H. Hu, X. Wang, J. Wang, L. Wan, F. Liu, H. Zheng, et al., Chem. Phys. Lett. 484 (2010) 247–253.
[132] Y. Huang, Y. Qin, Y. Zhou, H. Niu, Z.-Z. Yu, J.-Y. Dong, Chem. Mater. 22 (2010) 4096–4102.
[133] G.-H. Chen, D.-J. Wu, W.-G. Weng, W.-L. Yan, J. Appl. Polym. Sci. 82 (2001) 2506–2513.
[134] F. Leroux, J.-P. Besse, Chem. Mater. 13 (2001) 3507–3515.
[135] N.I. Kovtyukhova, P.J. Ollivier, B.R. Martin, T.E. Mallouk, S.A. Chizhik, E.V. Buzaneva, et al., Chem. Mater. 11 (1999) 771–778.
[136] D.D. Kulkarni, I. Choi, S.S. Singamaneni, V.V. Tsukruk, ACS Nano 4 (2010) 4667–4676.
[137] N.A. Kotov, I. Dékány, J.H. Fendler, Adv. Mater. 8 (1996) 637–641.
[138] M. Yang, Y. Hou, N.A. Kotov, Nano Today 7 (2012) 430–447.
[139] X. Zhao, Q. Zhang, D. Chen, P. Lu, Macromolecules 43 (2010) 2357–2363.
[140] J.J. Richardson, M. Björnmalm, F. Caruso, Science (2015) 348.
[141] D.A. Dikin, S. Stankovich, E.J. Zimney, R.D. Piner, G.H.B. Dommett, G. Evmenenko, et al., Nature 448 (2007) 457–460.
[142] G. Eda, G. Fanchini, M. Chhowalla, Nat. Nanotechnol. 3 (2008) 270–274.
[143] H. Chen, M.B. Müller, K.J. Gilmore, G.G. Wallace, D. Li, Adv. Mater. 20 (2008) 3557–3561.
[144] Y. Zhang, S. Gong, Q. Zhang, P. Ming, S. Wan, J. Peng, et al., Chem. Soc. Rev. 45 (2016) 2378–2395.
[145] W. Cui, M. Li, J. Liu, B. Wang, C. Zhang, L. Jiang, et al., ACS Nano 8 (2014) 9511–9517.
[146] N. Zhao, M. Yang, Q. Zhao, W. Gao, T. Xie, H. Bai, ACS Nano 11 (2017) 4777–4784.
[147] H. Cheng, C. Hu, Y. Zhao, L. Qu, NPG Asia Mater. 6 (2014) e113.
[148] Z. Xu, C. Gao, Acc. Chem. Res. 47 (2014) 1267–1276.
[149] F. Meng, W. Lu, Q. Li, J.-H. Byun, Y. Oh, T.-W. Chou, Adv. Mater. 27 (2015) 5113–5131.
[150] G. Xin, T. Yao, H. Sun, S.M. Scott, D. Shao, G. Wang, et al., Science 349 (2015) 1083–1087.
[151] Z. Xu, Y. Liu, X. Zhao, L. Peng, H. Sun, Y. Xu, et al., Adv. Mater. 28 (2016) 6449–6456.
[152] K. Batrakov, P. Kuzhir, S. Maksimenko, A. Paddubskaya, S. Voronovich, P. Lambin, et al., Sci. Rep. 4 (2014).
[153] I. Vlassiouk, G. Polizos, R. Cooper, I. Ivanov, J.K. Keum, F. Paulauskas, et al., ACS Appl. Mater. Interfaces 7 (2015) 10702–10709.
[154] X. Zhang, P. Samorì, Angew. Chem. Int. Ed. 55 (2016) 15472–15474.
[155] H.J. Park, J. Meyer, S. Roth, V. Skákalová, Carbon 48 (2010) 1088–1094.
[156] Y. Kim, J. Lee, M.S. Yeom, J.W. Shin, H. Kim, Y. Cui, et al., Nat. Commun. 4 (2013) 2114.
[157] M. Kolle, A. Lethbridge, M. Kreysing, J.J. Baumberg, J. Aizenberg, P. Vukusic, Adv. Mater. 25 (2013) 2239–2245.
[158] S. Park, Nat. Rev. Mater. 1 (2016) 16085.
[159] S. Bae, H. Kim, Y. Lee, X. Xu, J.-S. Park, Y. Zheng, et al., Nat. Nanotechnol. 5 (2010) 574–578.
[160] T. Kobayashi, M. Bando, N. Kimura, K. Shimizu, K. Kadono, N. Umezu, et al., Appl. Phys. Lett. 102 (2013) 023112.
[161] C.S. Ruiz-Vargas, H.L. Zhuang, P.Y. Huang, A.M. van der Zande, S. Garg, P.L. McEuen, et al., Nano Lett. 11 (2011) 2259–2263.
[162] Q.-Y. Lin, G. Jing, Y.-B. Zhou, Y.-F. Wang, J. Meng, Y.-Q. Bie, et al., ACS Nano 7 (2013) 1171–1177.
[163] A.A. RamanathanT, Abdala, D.A. StankovichS, M. Dikin, R.D. Herrera Alonso, Piner, et al., Nat. Nanotechnol. 3 (2008) 327–331.
[164] M.A. Rafiee, J. Rafiee, Z. Wang, H. Song, Z.-Z. Yu, N. Koratkar, ACS Nano 3 (2009) 3884–3890.
[165] B. Ramezanzadeh, E. Ghasemi, M. Mahdavian, E. Changizi, M.H. Mohamadzadeh Moghadam, Chem. Eng. J. 281 (2015) 869–883.
[166] Y. Zhu, H. Wang, J. Zhu, L. Chang, L. Ye, Appl. Surf. Sci. 349 (2015) 27–34.
[167] S.B. Kadambi, K. Pramoda, U. Ramamurty, C.N.R. Rao, ACS Appl. Mater. Interfaces 7 (2015) 17016–17022.
[168] S. Roy, X. Tang, T. Das, L. Zhang, Y. Li, S. Ting, et al., ACS Appl. Mater. Interfaces 7 (2015) 3142–3151.
[169] K.-H. Liao, S. Aoyama, A.A. Abdala, C. Macosko, Macromolecules 47 (2014) 8311–8319.
[170] J.W. Suk, R.D. Piner, J. An, R.S. Ruoff, ACS Nano 4 (2010) 6557–6564.
[171] X. Li, G.B. McKenna, ACS Macro Lett. 1 (2012) 388–391.
[172] D.H. Droste, A.T. Dibenedetto, J. Appl. Polym. Sci. 13 (1969) 2149–2168.
[173] E.D. Wetzel, R. Balu, T.D. Beaudet, J. Mech. Phys. Solids 82 (2015) 23–31.
[174] P. Liu, M.S. Strano, Adv. Funct. Mater. 26 (2016) 943–954.
[175] T. Jiang, R. Huang, Y. Zhu, Adv. Funct. Mater. 24 (2014) 396–402.
[176] R.J. Young, L. Gong, I.A. Kinloch, I. Riaz, R. Jalil, K.S. Novoselov, ACS Nano 5 (2011) 3079–3084.
[177] S.L. Phoenix, P.K. Porwal, Int. J. Solids Struct. 40 (2003) 6723–6765.
[178] K. Choi, S. Nam, Y. Lee, M. Lee, J. Jang, S.J. Kim, et al., ACS Nano 9 (2015) 5818–5824.
[179] S. Seethamraju, S. Kumar, K.B.B, G. Madras, S. Raghavan, P.C. Ramamurthy, ACS Nano 10 (2016) 6501–6509.
[180] B. Wang, B.V. Cunning, S.-Y. Park, M. Huang, J.-Y. Kim, R.S. Ruoff, ACS Nano 10 (2016) 9794–9800.
[181] M.H. Wong, J.P. Giraldo, S.-Y. Kwak, V.B. Koman, R. Sinclair, T.T.S. Lew, et al., Nat. Mater. 16 (2017) 264–272.
[182] J.P. Giraldo, M.P. Laundry, S.M. Faltermeier, T.P. McNicholas, N.M. Iverson, A.A. Boghossian, N.F. Rueul, A.J. Hilmer, F. Sen, J.A. Brew, M.S. Strano, Nat. Mater. (2014) 13.
[183] A. Yializis, G.L. Powers, D.G. Shaw, 40th Conf. Proc. Electron. Compon. Technol. 1990, pp. 169–176 vol. 161.
[184] R.P. Almazán, L. Pérez, C. Aroca, M.C. Sánchez, E. López, P. Sánchez, J. Magn. Magn. Mater. 254 (2003) 630–632.
[185] D.J. Sadler, S. Gupta, C.H. Ahn, IEEE Trans. Magn. 37 (2001) 2897–2899.
[186] W.A. Roshen, D.E. Turcotte, IEEE Trans. Magn. 24 (1988) 3213–3216.
[187] T.M. Liakopoulos, C.H. Ahn, IEEE Trans. Magn. 35 (1999) 3679–3681.
[188] I. Vincueria, M. Tudanca, C. Aroca, E. Lopez, M.C. Sanchez, P. Sanchez, IEEE Trans. Magn. 30 (1994) 5042–5045.
[189] J.M. Azzarelli, K.A. Mirica, J.B. Ravnsbæk, T.M. Swager, Proc. Natl. Acad. Sci. U. S. A. 111 (2014) 18162–18166.
[190] M.S. Mannoor, H. Tao, J.D. Clayton, A. Sengupta, D.L. Kaplan, R.R. Naik, et al., Nat. Commun. 3 (2012) 763.
[191] W. Honda, S. Harada, T. Arie, S. Akita, K. Takei, Adv. Funct. Mater. 24 (2014) 3299–3304.
[192] S. Xu, Z. Yan, K.I. Jang, W. Huang, H.R. Fu, J. Kim, et al., Science 347 (2015) 154–159.
[193] Z. Yan, F. Zhang, F. Liu, M.D. Han, D.P. Ou, Y.H. Liu, et al., Sci. Adv. (2016) 2.
[194] P. Ripka, J. Magn. Magn. Mater. 215 (2000) 735–739.
[195] S.O. Choi, S. Kawahito, Y. Matsumoto, M. Ishida, Y. Tadokoro, Sens. Actuators A 55 (1996) 121–126.
[196] P. Ripka, S. Kawahito, S.O. Choi, A. Tipek, M. Ishida, Sens. Actuators A 91 (2001) 65–69.
[197] S. Kawahito, Y. Sasaki, H. Sato, T. Nakamura, Y. Tadokoro, Sens. Actuators A 43 (1994) 128–134.
[198] T.M. Liakopoulos, C.H. Ahn, Sens. Actuators A 77 (1999) 66–72.
[199] L. Perez, C. Aroca, P. Sánchez, E. López, M.C. Sánchez, Sens. Actuators A 109 (2004) 208–211.
[200] D. Seo, R.M. Neely, K. Shen, U. Singhal, E. Alon, J.M. Rabaey, et al., Neuron 91 (2016) 529–539.
[201] D. Seo, J.M. Carmena, J.M. Rabaey, M.M. Maharbiz, E. Alon, J. Neurosci. Methods 244 (2015) 114–122.

Please cite this article in press as: P. Liu, et al., Emerging trends in 2D nanotechnology that are redefining our understanding of "Nanocomposites", Nano Today (2018), https://doi.org/10.1016/j.nantod.2018.04.012

[202] A. Zebda, S. Cosnier, J.P. Alcaraz, M. Holzinger, A. Le Goff, C. Gondran, et al., Sci. Rep. 3 (2013) 1516.
[203] H. Kim, M.J. Kim, IEEE Trans. Robot. 32 (2016) 125–137.
[204] A. Servant, F. Qiu, M. Mazza, K. Kostarelos, B.J. Nelson, Adv. Mater. 27 (2015) 2981–2988.
[205] S.T. Chang, V.N. Paunov, D.N. Petsev, O.D. Velev, Nat. Mater. 6 (2007) 235–240.
[206] G.A. Salvatore, N. Münzenrieder, T. Kinkeldei, L. Petti, C. Zysset, I. Strebel, et al., Nat. Commun. 5 (2014) 2982.
[207] D. Akinwande, N. Petrone, J. Hone, Nat. Commun. 5 (2014) 5678.
[208] P. Goli, S. Legedza, A. Dhar, R. Salgado, J. Renteria, A.A. Balandin, J. Power Sources 248 (2014) 37–43.
[209] V. Goyal, A.A. Balandin, Appl. Phys. Lett. 100 (2012) 073113.
[210] H. Malekpour, K.H. Chang, J.C. Chen, C.Y. Lu, D.L. Nika, K.S. Novoselov, et al., Nano Lett. 14 (2014) 5155–5161.
[211] S. Ramirez, K. Chan, R. Hernandez, E. Recinos, E. Hernandez, R. Salgado, et al., Mater. Des. 118 (2017) 75–80.
[212] J. Renteria, S. Legedza, R. Salgado, M.P. Balandin, S. Ramirez, M. Saadah, et al., Mater. Des. 88 (2015) 214–221.
[213] J. Renteria, D. Nika, A. Balandin, Appl. Sci. 4 (2014) 525.
[214] J.D. Renteria, S. Ramirez, H. Malekpour, B. Alonso, A. Centeno, A. Zurutuza, et al., Adv. Funct. Mater. 25 (2015) 4664–4672.
[215] M. Saadah, E. Hernandez, A. Balandin, Appl. Sci. 7 (2017) 589.
[216] E. Pop, V. Varshney, A.K. Roy, MRS Bull. 37 (2012) 1273–1281.
[217] J.P. Dowling, M. Scalora, M.J. Bloemer, C.M. Bowden, J. Appl. Phys. 75 (1994) 1896–1899.
[218] K.V. Sreekanth, S. Zeng, J. Shang, K.T. Yong, T. Yu, Sci. Rep. 2 (2012) 737.
[219] K.V. Sreekanth, S. Zeng, K.-T. Yong, T. Yu, Sens. Actuators, B 182 (2013) 424–428.
[220] D.G. Figueroa del Valle, E. Aluicio-Sarduy, F. Scotognella, Opt. Mater. 48 (2015) 267–270.
[221] H. Yan, X. Li, B. Chandra, G. Tulevski, Y. Wu, M. Freitag, et al., Nat. Nanotechnol. 7 (2012) 330–334.
[222] P. Michler, A. Imamoğlu, M. Mason, P. Carson, G. Strouse, S. Buratto, Nature 406 (2000) 968–970.
[223] A. Högele, C. Galland, M. Winger, A. Imamoğlu, Phys. Rev. Lett. 100 (2008) 217401.
[224] T.M. Babinec, B.J. Hausmann, M. Khan, Y. Zhang, J.R. Maze, P.R. Hemmer, et al., Nat. Nanotechnol. 5 (2010) 195–199.
[225] C. Kurtsiefer, S. Mayer, P. Zarda, H. Weinfurter, Phys. Rev. Lett. 85 (2000) 290–293.
[226] A. Srivastava, M. Sidler, A.V. Allain, D.S. Lembke, A. Kis, A. Imamoglu, Nat. Nanotechnol. (2015).
[227] M. Koperski, K. Nogajewski, A. Arora, V. Cherkez, P. Mallet, J.Y. Veuillen, et al., Nat. Nanotechnol. 10 (2015) 503–506.
[228] Y.M. He, G. Clark, J.R. Schaibley, Y. He, M.C. Chen, Y.J. Wei, et al., Nat. Nanotechnol. 10 (2015) 497–502.
[229] A.W. Schell, H. Takashima, T.T. Tran, I. Aharonovich, S. Takeuchi, ACS Nano 4 (2017) 761–767.
[230] T.T. Tran, D. Wang, Z.Q. Xu, A. Yang, M. Toth, T.W. Odom, et al., Nano Lett. 17 (2017) 2634–2639.
[231] S. Dufferwiel, S. Schwarz, F. Withers, A.A. Trichet, F. Li, M. Sich, et al., Nat. Commun. 6 (2015) 8579.
[232] Y. Ye, Z.J. Wong, X. Lu, X. Ni, H. Zhu, X. Chen, et al., Nat. Photonics 9 (2015) 733–737.
[233] S. Wu, S. Buckley, J.R. Schaibley, L. Feng, J. Yan, D.G. Mandrus, et al., Nature 520 (2015) 69–72.
[234] T.T. Tran, K. Bray, M.J. Ford, M. Toth, I. Aharonovich, Nat. Nanotechnol. 11 (2016) 37–41.
[235] I. Aharonovich, D. Englund, M. Toth, Nat. Photonics 10 (2016) 631–641.
[236] S. Choi, T.T. Tran, C. Elbadawi, C. Lobo, X. Wang, S. Juodkazis, et al., ACS Appl. Mater. Interfaces 8 (2016) 29642–29648.
[237] N. Chejanovsky, M. Rezai, F. Paolucci, Y. Kim, T. Rendler, W. Rouabeh, et al., Nano Lett. 16 (2016) 7037–7045.
[238] Z.-Q. Xu, C. Elbadawi, T.T. Tran, M. Kianinia, T.B. Hoffman, J.H. Edgar, et al., arXiv: 1704.05154, (2017).
[239] T.T. Tran, C. Elbadawi, D. Totonjian, C.J. Lobo, G. Grosso, H. Moon, et al., ACS Nano 10 (2016) 7331–7338.
[240] G. Grosso, H. Moon, B. Lienhard, S. Ali, D.K. Efetov, M.M. Furchi, et al., Nat. Commun. (2017) 8.
[241] F. Dolde, H. Fedder, M.W. Doherty, T. Nöbauer, F. Rempp, G. Balasubramanian, et al., Nat. Phys. 7 (2011) 459–463.
[242] P. Neumann, I. Jakobi, F. Dolde, C. Burk, R. Reuter, G. Waldherr, et al., Nano Lett. 13 (2013) 2738–2742.
[243] V.N. Mochalin, O. Shenderova, D. Ho, Y. Gogotsi, Nat. Nanotechnol. 7 (2011) 11–23.
[244] L.P. McGuinness, Y. Yan, A. Stacey, D.A. Simpson, L.T. Hall, D. Maclaurin, et al., Nat. Nanotechnol. 6 (2011) 358–363.
[245] C.T. Kenry, Lim, ChemNanoMat 3 (2017) 5–16.
[246] J. Slegerova, M. Hajek, I. Rehor, F. Sedlak, J. Stursa, M. Hruby, et al., Nanoscale 7 (2015) 415–420.
[247] I. Rehor, H. Mackova, S.K. Filippov, J. Kucka, V. Proks, J. Slegerova, et al., ChemPlusChem 79 (2014) 21–24.
[248] T. Rendler, J. Neburkova, O. Zemek, J. Kotek, A. Zappe, Z. Chu, et al., Nat. Commun. 8 (2017) 14701.
[249] F.J. Clauss, Solid Lubricants and Self-Lubricating Solids, Elsevier, 2012.
[250] W. Ren, H.-M. Cheng, Nat. Nanotechnol. 9 (2014) 726–730.
[251] J.W. Colson, W.R. Dichtel, Nat. Chem. 5 (2013) 453–465.
[252] C.E. Boott, A. Nazemi, I. Manners, Angew. Chem. Int. Ed. 54 (2015) 13876–13894.
[253] N.A.A. Zwaneveld, R. Pawlak, M. Abel, D. Catalin, D. Gigmes, D. Bertin, et al., J. Am. Chem. Soc. 130 (2008) 6678–6679.
[254] J.W. Colson, A.R. Woll, A. Mukherjee, M.P. Levendorf, E.L. Spitler, V.B. Shields, et al., Science 332 (2011) 228–231.
[255] D.J. Murray, D.D. Patterson, P. Payamyar, R. Bhola, W. Song, M. Lackinger, et al., J. Am. Chem. Soc. 137 (2015) 3450–3453.
[256] W. Dai, F. Shao, J. Szczerbiński, R. McCaffrey, R. Zenobi, Y. Jin, et al., Angew. Chem. 128 (2016) 221–225.
[257] H. Sahabudeen, H. Qi, B.A. Glatz, D. Tranca, R. Dong, Y. Hou, et al., Nat. Commun. 7 (2016) 13461.
[258] P. Kissel, R. Erni, W.B. Schweizer, M.D. Rossell, B.T. King, T. Bauer, et al., Nat. Chem. 4 (2012) 287–291.
[259] P. Kissel, D.J. Murray, W.J. Wulftange, V.J. Catalano, B.T. King, Nat. Chem. 6 (2014) 774–778.
[260] R.Z. Lange, G. Hofer, T. Weber, A.D. Schlüter, J. Am. Chem. Soc. 139 (2017) 2053–2059.
[261] W. Liu, X. Luo, Y. Bao, Y.P. Liu, G.-H. Ning, I. Abdelwahab, et al., Nat. Chem. 9 (2017) 563–570.
[262] D.N. Bunck, W.R. Dichtel, J. Am. Chem. Soc. 135 (2013) 14952–14955.
[263] P. Sun, R. Ma, X. Bai, K. Wang, H. Zhu, T. Sasaki, Sci. Adv. 3 (2017) e1602629.
[264] P. Sun, R. Ma, T. Sasaki, Chem. Sci. 9 (2018) 33–43.

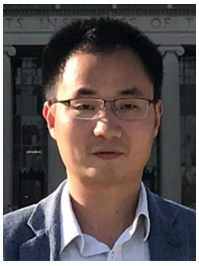

Dr. Pingwei Liu is currently an Assistant Professor of Chemical and Biological Engineering at Zhejiang University, China. He received his PhD degree from the State Key Laboratory of Chemical Engineering at Zhejiang University in 2014. He conducted postdoctoral research at Massachusetts Institute of Technology (MIT) in the group of Prof. Michael Strano. His research interests include the synthesis and characterization of polymers and nanomaterials as well as the study of their applications in nanocomposites, catalysis, and sensors.

Anton Cottrill is a Ph.D. candidate in Prof. Michael Strano's research group in the Department of Chemical Engineering at MIT. His Ph.D. thesis has focused primarily on material and device development for thermal energy harvesting and thermal energy conservation.

Dr. Daichi Kozawa received his M.Sc. in Energy Science from Kyoto University in 2012 and Ph.D. in the same discipline from the same University in 2015. The same year he became a JSPS Postdoctoral Fellow of the Japan Society for the Promotion of Science and worked at Waseda University. Dr. Kozawa joined Strano Research Group at Massachusetts Institute of Technology as a postdoctoral fellow in 2015. The focuses of his project are on the optical application of 2D material/polymer composites and spectroscopic study of 2D materials and their nanoscale defects

Dr. Volodymyr Koman received his BS in Applied Physics from Ivan Franko National University in Ukraine. He did his PhD at EPFL, Switzerland where he developed portable sensors for nanotoxicology studies. He is currently a Swiss NSF PostDoctoral Fellow at Chemical Engineering, MIT, where he focuses on 2D materials, nanosensors, and plant nanobionics.

Please cite this article in press as: P. Liu, et al., Emerging trends in 2D nanotechnology that are redefining our understanding of "Nanocomposites", Nano Today (2018), https://doi.org/10.1016/j.nantod.2018.04.012

Dr. Dorsa Parviz received her B.Sc. in Chemical Engineering from Amirkabir University of Technology and her M.Sc. from Sharif University of Technology, where she conducted research on nanocatalysts synthesis. In 2016, she received her Ph.D. in Chemical Engineering from Texas A&M University. She joined Strano Research Group at Massachusetts Institute of technology for her postdoctoral studies in 2017. Her research focuses on processing and applications of colloidal 2D materials, their polymer nanocomposites, and porous conductive networks.

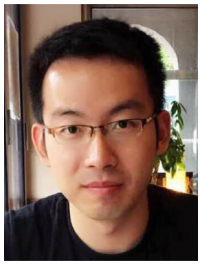

Albert Tianxiang Liu obtained his bachelor's degree in Chemical Engineering from California Institute of Technology and is currently working on his PhD with Prof. Michael S. Strano at Massachusetts Institute of Technology. Prior to joining MIT as a graduate fellow, Albert had studied physical organic chemistry and organometallic chemistry under the tutelage of Prof. John D. Roberts and Prof. Gregory C. Fu, and had spent a summer at Chevron Co. learning zeolite synthesis from Dr. Stacey I. Zones. His research interests include the analysis and control of molecular conformation and engineering of low dimensional materials with applications in chemical transformation and energy generation.

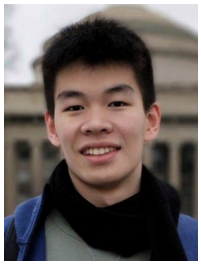

Jing Fan Yang is a PhD student in Professor Michael Strano's group at Department of Chemical Engineering, Massachusetts Institute of Technology. He completed his B.Eng. in Chemical and Biomolecular Engineering at Nanyang Technological University, Singapore. His current research interests include modelling and fabrication of colloidal state machines.

Thang Q. Tran received his bachelor's honor degree in Mechanical Engineering in 2009 from the Ho Chi Minh City University of Technology (Bach Khoa University), Vietnam. Currently, he is a PhD candidate in Assoc. Prof. Duong Hai Minh's research group at the Carbon-based Nanoengineering Materials Laboratory, Department of Mechanical Engineering, National University of Singapore. His current research interests include carbon nanotube/graphene composite fibers, conducting cables/wires, and smart textiles.

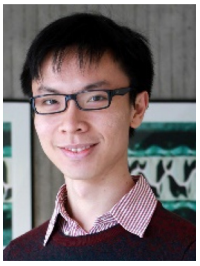

Min Hao Wong is currently a Chemical Engineering graduate student at MIT. His PhD research involved the development of unique nanosensor applications for agriculture. His work has been published in Nature Mater., Nanolett etc, and featured in global media outlets such as FOX, Forbes, TIME, BBC, and CBS. BostInno named his work as one of the top 7 inventions to come out of MIT in 2016. Min Hao is also currently actively running Plantea, a start-up company focused on agricultural nanosensors. He is also the deputy scientific director of DiSTAP (Center for Disruptive and Sustainable Technologies for Agricultural Precision – Singapore) and a guest lecturer for 10.585 Engineering Nanotechnology.

Song Wang graduated from Zhejiang University with a bachelor degree of Chemical Engineering in 2013. He is currently finishing his Ph.D. degree in Chemical Engineering at Zhejiang University. His research focus on functional polymer, covalent organic framework and thermal engineering.

Professor Michael S. Strano is currently the Carbon P. Dubbs Professor of Chemical Engineering at the Massachusetts Institute of Technology. He received his B.S from Polytechnic University in Brooklyn, NY and Ph.D. from the University of Delaware both in Chemical Engineering. He was a post doctoral research fellow at Rice University in the departments of Chemistry and Physics under the guidance of Nobel Laureate Richard E. Smalley. From 2003 to 2007, Michael was an Assistant Professor in the Department of Chemical and Biomolecular Engineering at the University of Illinois at Urbana- Champaign before moving to MIT. His research focuses on biomolecule/nanoparticle interactions and the surface chemistry of low dimensional systems, nano-electronics, nanoparticle separations, and applications of vibrational spectroscopy to nanotechnology. Michael recently completed a two year commitment with the Defense Science Study Group (DSSG) and is a current member of the Defense Science Board (DSB). He is the recipient of numerous awards for his work from 2005 to the present, including being recently named one of the world's most influential scientific minds by Thomson Reuters and elected to the National Academy of Engineering.

Please cite this article in press as: P. Liu, et al., Emerging trends in 2D nanotechnology that are redefining our understanding of "Nanocomposites", Nano Today (2018), https://doi.org/10.1016/j.nantod.2018.04.012